TAMPEREEN TEKNILLINEN YLIOPISTO
TAMPERE UNIVERSITY OF TECHNOLOGY

Padma Bolla

Advanced Tracking Loop Architectures for Multi-frequency GNSS Receiver

Julkaisu 1609 • Publication 1609

Tampere 2018

SAMARA UNIVERSITY
Samara National Research University

Tampereen teknillinen yliopisto. Julkaisu 1609
Tampere University of Technology. Publication 1609

Padma Bolla

Advanced Tracking Loop Architectures for Multi-frequency GNSS Receiver

Thesis for the degree of Doctor of Science in Technology to be presented with due permission for public examination and criticism in Rakennustalo Building, Auditorium RG202, at Tampere University of Technology, on the 17th of December 2018, at 12 noon.

Tampereen teknillinen yliopisto - Tampere University of Technology
Samara National Research University
Tampere 2018

Doctoral candidate: Padma Bolla
Faculty of Computing and Electrical Engineering
Tampere University of Technology, Finland
Faculty of Electronics and Instrument Engineering
Samara National Research University, Russia

Supervisors: Elena-Simona Lohan, Associate Professor
Laboratory of Electronics and Communications Engineering
Faculty of Computing and Electrical Engineering
Tampere University of Technology
Finland

Jari Nurmi, Professor
Laboratory of Electronics and Communications Engineering
Faculty of Computing and Electrical Engineering
Tampere University of Technology
Finland

Ilya Kudryavtsev, Dean
Faculty of Electronics and Instrument Engineering
Samara National Research University
Russia

Pre-examiners: Pratap Misra, Professor
Mechanical Engineering
Tufts University
Medford, USA

Daniele Borio, PhD
Scientific and Technical Officer
Joint Research Centre (JRC) of the European Commission
Ispra, Italy

Opponents: Thomas Pany, Univ.-Prof. Mag. Dr. habil
Department of Aerospace Engineering
University of the Federal Armed Forces Munich
Neubiberg, Germany

Octavian Thor Pleter, Professor, Dean, PhD, PhD, MBA (MBS)
Faculty of Aerospace Engineering
University Politehnica of Bucharest
Bucharest, Romania

Igor V. Belokonov, Professor
Head of Inter-University Space Research Department
Samara National Research University
Samara, Russia

ISBN 978-952-15-4288-6 (printed)
ISBN 978-952-15-4309-8 (PDF)
ISSN 1459-2045

Abstract

The multi-frequency Global Navigation Satellite System (GNSS) signals are designed to overcome the inherent performance limitations of single-frequency receivers. However, the processing of multiple frequency signals in a time-varying GNSS signal environment which are potentially affected by multipath, ionosphere scintillation, blockage, and interference is quite challenging, as each signal is influenced differently by channel effects according to its Radio Frequency (RF). In order to get benefit of synchronously/coherently generated multiple frequency signals, advanced receiver signal processing techniques need to be developed.

The aim of this research thesis is to extract the best performance benefits out of multi-frequency GNSS signals in a time-varying GNSS signal environment. To accomplish this objective, it is necessary to analyze the multi-frequency signal characteristics and to investigate suitable signal processing algorithms in order to enable the best performance of each signal. The GNSS receiver position accuracy and reliability are majorly determined by the signal tracking-loop performance, hence, the primary focus of this thesis is on improving the tracking-loop performance of coherently generated multi-frequency signals.

In the first phase of this research, the performance of multi-frequency GNSS signals is analyzed using conventional signal processing algorithms. Furthermore, the performance of a combination of multi-frequency signals is evaluated in order to find the optimum two-frequency signal combination for standalone and differential positioning applications. The limitations of the conventional multi-frequency signal processing algorithms are identified and an optimum dual-frequency signal processing architecture is proposed for robust and precise positioning applications.

By making use of the inherent linear relation between the Line-of-Sight (LOS) Doppler shifts of multi-frequency GNSS signals, a computationally efficient Centralized Dynamics Tracking Loop (CTL) architecture is also proposed. In the CTL architecture, the common geometric Doppler shift in the received multi-frequency signals is estimated using a higher-order wide-band filter by making use of multiple frequency channel measurements in a coordinated manner. Additionally, the residual-phase variations specific to each frequency channel are tracked using Phase Lock Loop (PLL) with a narrow bandwidth filter. The CTL filter provides the geometric Doppler shift aid to individual frequency channels. The common Doppler-aided narrow-band signal tracking enhances the signal tracking sensitivity and robustness to the in-band interference in each frequency channel. This further reduces the noise in the linear combination of pseudorange observations.

In real GNSS signal environment, multiple frequency signals are often subjected to intentional or unintentional RF interference either at the same time or at different time instants. Moreover, each of these signals is influenced differently by RF interference. To track signals in such time-varying signal conditions, the CTL using an Adaptive

Kalman Filter (AKF) is proposed to enable an adaptive tracking loop bandwidth in response to received signal power level and signal dynamics. The central task of the AKF is to effectively blend multiple frequency carrier-phase observations to estimate the common geometric Doppler frequency of received multiple frequency signals. A suitable collaboration in multi-frequency channel tracking using centralized dynamics tracking loop enables a robust carrier tracking even if some of the frequency channels are affected by ionospheric scintillation, multipath, or interference.

The performance of the proposed multi-frequency GNSS signal processing algorithms is demonstrated using analytical methods and experimental results based on live satellite data collected over GPS L1, L2C, and L5 signal frequencies. The dual-frequency signal processing architecture proposed in this research thesis has reduced the position error by 50%. The centralized dynamics multi-frequency carrier tracking loop has enhanced the individual channel tracking loop threshold by 7 dB in challenging signal conditions.

Preface

First of all, my profound gratitude and reverence to God Almighty for being the pillar of strength through this journey.

This research thesis was inspired by the vision of Prof. Kai Borre (of blessed memory) and encouraged by other outstanding people. I would like to extend my eternal gratitude to Prof. Kai Borre. My sincere thanks to the institutions, professors and all those who helped in the actualization of this research thesis.

First, I would like to thank the team at Samara National Research University, Russia, for assimilating me into their GNSS laboratory facilities and resources which played a vital role to this research thesis. Special acknowledgements are due to:
- Ilya Kudryavtsev, Dean of Faculty of Electronics and Instrument Engineering, who has been so supportive throughout this process.
- Stepan Shafran, for his kind help in collecting live satellite data whenever required and being patient in listening to my research discussions. Anna Stepashkina, Ekaterina Gizatulova and the staff of international department who made me feel at home in Russia despite the language barrier.

Then, I would like to thank the team at Tampere University of Technology, Finland, for the seamless effort to create the synthesis of my thoughts and ideas. My sincere gratitude to Assoc. Prof. Elena-Simona Lohan and Prof. Jari Nurmi, for your continuous support, patience, and wise guidance. Your warmth and willingness to take me in served as a source of strength in dire moments. You have played a key role in establishing the harmonious collaboration between the SSAU and TUT to carry out research in GNSS technology.

I would like to thank the team at Inha University, South Korea, for the warm reception of my ideas. Unreserved gratitude goes to Assoc. Prof. Jong-Hoon Won, who accommodated me as an intern for a period of five months to carry out my research. To all the amazing students of GNSS lab who made my stay in South Korea a memorable experience.

I am grateful to Prof. Pratap Misra and Dr. Daniele Borio to act as the pre-examiners of my thesis and for their constructive feedback. I also wish to thank Prof. Thomas Pany and Prof. Octavian Thor Pleter, for agreeing to act as the opponents at my defense.

In addition, I also want to thank my employer and colleagues in Defense Research and Development Organization, India, for granting permission and three years of sabbatical leave to pursue my Doctoral studies.

Last but not least, I am indebted to my beloved family members and friends, for their unconditional love and encouragement to pursue my passions. This work would not have been possible without their support.

Contents

Acronyms

AKF	Adaptive Kalman Filter
ARNS	Aeronautical Radio Navigation Service
AWGN	Additive White Gaussian Noise
BLWN	Band Limited White Noise
BW	Bandwidth
COTS	Commercial-Off-The-Shelf
CTL	Centralized Dynamics Tracking Loop
CW	Continuous Wave
DF	Divergence-free
DFS	Divergence-free smoothed pseudorange
DGPS	Differential GPS
DLL	Delay Lock Loop
DOP	Dilution of Position
DPLL	Digital Phase Lock Loop
EGNOS	European Geostationary Navigation Overlay Service
FLL	Frequency Lock Loop
F-PLL	FLL-assisted Phase Locked Loop
GAGAN	GPS-Aided GEO Augmented Navigation
GNSS	Global Navigation Satellite System
GPS	Global Positioning System
HDOP	Horizontal Dilution of Precision
IAR	Integer Ambiguity Resolution
IFS	Ionosphere-free smoothed pseudorange
IF	Intermediate Frequency

INS Inertial Navigation System

IoT Internet of Things

KF Kalman Filter

LBS Location Based Services

LOS Line-of-Sight

MEE Multipath Error Envelope

MMSE Minimum Mean Square Error

MSAS Multi-functional Satellite Augmentation System

NCO Numerically Controlled Oscillator

NLS Narrow-lane carrier phase smoothed wide-lane pseudorange

PD Phase Discriminator

PDOP Position Dilution of Position

PIT Pre-detection Integration Time

PLL Phase Lock Loop

PPP Precise Point Positioning

RF Radio Frequency

RMS Root Mean Square

RNSS Regional Navigation Satellite System

SBAS Space Based Augmentation System

STL Scalar Tracking Loop

TCAR Three Carrier Ambiguity Resolution

TEC Total Electron Content

VPLL Vector Phase Lock Loop

VTL Vector Tracking Loop

WAAS Wide Area Augmentation System

WLS wide-lane carrier phase smoothed narrow-lane pseudorange

Nomenclature

C/A	Coarse Acquisition code
$s(t)$	Received signal
P_k	Received signal power in k-th channel
$C_k(t)$	Pseudo-random code in k-th channel
$D_k(t)$	Navigation message data bits in k-th channel
τ_k	Transition delay from satellite to the receiver in k-th channel
$f_{L_k}(t)$	Signal carrier frequency in k-th channel
$\phi_k(t)$	Signal carrier phase in k-th channel
$n_k(t)$	Noise in in k-th channel frequency band.
$\phi_0(t)$	Received signal phase
$\dot{\phi}_k(t)$	Carrier phase first time derivative in k-th channel
$\ddot{\phi}_k(t)$	Carrier phase second time derivative in k-th channel
ε_{ϕ_k}	Error in the carrier phase approximation in k-th channel
$f_{D_k}(t)$	Carrier Doppler frequency in k-th channel
$\dot{f}_{D_k}(t)$	Rate of carrier Doppler frequency in k-th channel
f_{GD_k}	Geometric Doppler shift in k-th channel
f_{RD_k}	Residual Doppler shift in k-th channel
f_{ID_k}	Ionospheric Doppler shift in k-th channel
f_{CD_k}	Reference clock Doppler shift in k-th channel
f_{L_k}	Carrier frequency of subscripted GPS L-band signals
f_{cL_k}	Code frequency of subscripted GPS L-band signals
λ_{cL_k}	Wavelength of the code frequency in k-th channel
λ_{L_k}	Wavelength of the carrier frequency in k-th channel
IE_k	Early In-phase correlator output of k-th frequency channel
QE_k	Early Quadrature phase correlator output of k-th channel
IP_k	Prompt In-phase correlator output of k-th channel
QP_k	Prompt Quadrature phase correlator output of k-th channel
IL_k	Late In-phase correlator output of k-th channel
QL_k	Late Quadrature phase correlator output of k-th channel
e_{τ_k}	Code phase discriminator output of k-th channel
e_{ϕ_k}	Carrier phase discriminator output of k-th channel
e_{f_k}	Frequency discriminator output of k-th channel
$\sigma_{\delta\tau}$	1-sigma code phase error
$\sigma_{\delta\phi}$	1-sigma carrier phase error
$\sigma_{\delta f}$	1-sigma frequency error
$\sigma_{\tau_{dll}}$	1-sigma thermal noise error in DLL
$\sigma_{\tau_{pll}}$	1-sigma thermal noise error in PLL
$\sigma_{\tau_{fll}}$	1-sigma thermal noise error in FLL

τ_e	1-sigma dynamic stress error in DLL
ϕ_e	1-sigma dynamic stress error in PLL
f_e	1-sigma dynamic stress error in FLL
B_{dll}	DLL loop bandwidth
B_{pll}	PLL loop bandwidth
B_{fll}	FLL loop bandwidth
T	Pre-detection integration time
s_g	Reference oscillator sensitivity factor
a_g	Acceleration dynamics
Q_J	Jamming resistance quality factor
R_c	Code rate of GNSS signal
C/N_0	Carrier-to-Noise ratio
$(C/N_0)_{eff}$	Effective Carrier-to-Noise ratio
$\Delta C/N_0$	Gain in C/N_0 signal tracking threshold
J/S	Jammer to Signal power ratio
ρ	Line-of-Sight geometric range
$\dot{\rho}$	Rate of geometric range
$\ddot{\rho}$	Acceleration of geometric range
I_k	Ionosphere delay in k-th channel
T_k	Troposphere delay in k-th channel
M_{P_k}	Multipath in code phase range observation in k-th channel
M_{ϕ_k}	Multipath in carrier phase range observation in k-th channel
γ_{ij}	Weight factor to code and carrier phase range observations
W_i	Weight factor to code phase range observations in Hatch filter
P_{SM}	Carrier smoothed code pseudorange observation
$\Delta\phi_k$	Carrier Doppler observation of k-th channel
ϕ_{WL}	Wide-lane carrier phase observations
$\hat{N}_{WL}$	Integer ambiguity estimate of wide-lane carrier phase observations
δI	Ionosphere delay bias
$\delta\mathbf{x}_t$	Error-state vector
F	Non-singular state transition matrix
H	Measurement matrix
Γ	Process noise gain vector
z_k	Phase error measurement in k-th channel
$\hat{z}_k$	Estimate of filtered residual phase measurement in k-th channel
q_t	Process noise acceleration variance
σ_{w_t}	Maximum acceleration increment over the sampling period
$\mathbf{z}_t$	Measurement vector at epoch
R_t	Measurement noise covariance matrix.
Q_t	Process noise covariance matrix.
$\tilde{\mathbf{z}}_t$	Innovation of the measurement vector
$\delta\hat{\mathbf{x}}_{t+1\|t}$	Predicted state vector
$\mathbf{P}_{t+1\|t}$	Prediction of state error covariance matrix
$\hat{\mathbf{C}}_{\tilde{\mathbf{z}}_t}$	Covariance of the innovation sequence
B_{eq}	Kalman filter equivalent noise bandwidth
c_n	Filter coefficient of n-th order PLL

List of Publications

P1. Padma Bolla and Kai Borre, "Performance analysis of dual-frequency receiver using combination of GPS L1, L5, and L2 civil signals," *Journal of Geodesy*, July 2018. https://doi.org/10.1007/s00190-018-1172-9. (**published**)

P2. Padma Bolla and Elena-Simona Lohan, "Dual-frequency signal processing architecture for robust and precise positioning applications," *in Proceedings of the IEEE/ION PLANS 2018*, Monterey, CA, April 2018, pp. 72-80. doi: 10.1109/PLANS.2018.8373367. (**published**)

P3. Padma Bolla, Jari Nurmi, Jong-Hoon Won and Elena-Simona Lohan, "Joint Tracking of Multiple Frequency Signals from the same GNSS Satellite", *in Proceedings of the IEEE /ICL-GNSS 2018*, Guimaraes, Portugal, June 2018, pp. 1-6, doi:10.1109/ICL-GNSS.2018.8440906. (**published**)

P4. Padma Bolla and Jong-Hoon Won, "Performance analysis of geometry-free and ionosphere-free code-carrier phase observation models in integer ambiguity resolution", *IET Radar, Sonar and Navigation*, Aug 2018, doi: 10.1049/iet-rsn.2018.5036. (**published**)

P5. Padma Bolla, Jordi Vila-Valls, Pau Closas and Elena-Simona Lohan, "Centralized Dynamics Multi-frequency GNSS Carrier Synchronization", *Institute of Navigation Journal*, 2018. (**Accepted**)

1 Introduction

Now we are living in an era of location-based services, such as mobile marketing, location of emergency calls, location-based information services, intelligent transportation, geo-tracking, autonomous-cars, Internet of Things (IoT), augmented reality and so on. Most of these services are enabled by the location information with different levels of performance requirements such as availability, accuracy, continuity, integrity, robustness, and authentication. For instance, augmented reality and autonomous navigation require high accuracy location information. The reliability is a critical parameter for safety-of-life applications and continuity of service is desirable in position tracking applications. No single technique or technology can serve a wide range of application requirements. Hence, most of today's Location Based Services (LBS) are realized using a synergy of technologies such as satellite-based positioning technology, cellular technologies, Internet, cloud processing, artificial intelligence, and so on. The position information in LBS is obtained using complementary positioning techniques, such as GNSS-based positioning for outdoor and cellular network-based positioning (2G, 3G, 4G, 5G), Bluetooth beacons, Wi-Fi base stations, or Inertial Navigation System (INS) for indoor positioning. A hybrid position solution will enable the availability of dynamic location information seamlessly both indoors and outdoors. Despite other alternative positioning technologies, GNSS-based positioning is widely used in the open sky/outdoors due to its global coverage, high accuracy, and free of service.

1.1 Background

GNSS is a satellite-based passive radio navigation technology that is capable of providing ubiquitous position, velocity, and time information. GNSS signals are transmitted by a constellation of satellites orbiting around the earth with global coverage. GNSS is the most cost-effective outdoor positioning technology currently available – which is serving a large scale of location-based applications. According to the GNSS market report [1], about 5.8 billion GNSS-based devices were in use in 2017. As many location-based services rely on position information, there is a stringent requirement for the accuracy, availability, and reliability of position information provided by the GNSS. Basically, the accuracy and reliability of GNSS-based positioning are influenced by two factors: the geometry of satellite constellation and the signal observation quality. The user-satellite geometry can be improved by the availability of a higher number of satellites through the integration of multiple constellations. The accuracy of GNSS signal observations is limited by many error sources such as satellite orbital parameter accuracy, satellite and receiver clock offsets, ionosphere and troposphere delays. Out of all these, the major source of observation errors is due to ionosphere delay incurred in the signal propagation path. In single-frequency receivers, ionosphere delay is estimated and

eliminated traditionally using either mathematical models or using corrections from augmentation services. In general, Klobuchar model for Global Positioning System (GPS) system [2] and NeQuick model for GALILEO system [3] are employed to correct ionosphere delay using broadcast parameters from satellites. These algorithms can be used in real-time and were designed to provide partial correction of the ionospheric range delay [4], [5]. Another alternative is to use corrections from either wide-area differential correction services or Space Based Augmentation System (SBAS) such as Wide Area Augmentation System (WAAS), European Geostationary Navigation Overlay Service (EGNOS), Multi-functional Satellite Augmentation System (MSAS) and GPS-Aided GEO Augmented Navigation (GAGAN) etc. However, the accuracy of the single-frequency receiver is limited due to the approximation and lack of tracking station coverage. The ionosphere delay in signal propagation path is frequency dispersive in nature [6], hence, the availability of two or more frequencies allows the receiver to form a linear combination of observations to estimate and eliminate common-mode ionosphere delay errors to improve the observation accuracy.

The changing trends and requirements of a wide range of location-based applications are the driving force for the evolution of GNSS infrastructure in the past decade. This drive has lead to the modernization of existed GPS (USA) and GLONASS (Russian Federation) systems with new civil signals and has recently launched GALILEO (Europian Union) and BeiDou (China) systems. These new systems are initialized with multiple frequency signals with advanced signal characteristics. Each of these systems has multiple civil signals in L1/L2/L5 frequency bands and they are designed to have one or more key advantages, suitable for different civilian applications. The four GNSSs and the two Regional Navigation Satellite Systems (RNSSs) i.e., QZSS (Japan) and NavIC (India) are transmitting signals over multiple frequencies. Both the regional and global systems are designed to be inter-operable and use the same frequency bands in the L−band spectrum, i.e., the spectrum in the $1-2\,\mathrm{GHz}$ band.

The objective of multi-frequency GNSS/RNSS signal transmission is three-fold:

- To serve diversified requirements of a wide spectrum of civilian applications. For instance, indoor positioning requires long-codes and high signal power to achieve higher signal sensitivity, while high dynamic applications need short-codes to enable fast signal acquisition and safety-of-life applications need RF carrier authentication to offer high integrity and reliability of position solution.
- To provide signal observations at multiple frequencies to enable to form a linear combination of observations used for different purpose. For instance, ionosphere-free combination, wide-lane combination, narrow-lane combination and so on.
- To improve the robustness of position solution through redundancy of multiple signal frequencies from the same satellite.

Now, the civilian user has a plethora of signals from multiple constellations. The availability of more signal choices will introduce another challenge to designers in justifying how many satellites and which of the multiple frequency signals are optimal for a given application. Significant research has been carried out in the past decade in analyzing the performance benefits of multi-frequency and multi-GNSS signals.

Integrated position solution using signals from two or more GNSS constellations improves the accuracy, availability, and robustness compared to single GNSS system. Naturally,

the integration of signals from more than one constellation increases the number of satellites. The large number of satellites in view may improve the accuracy through better geometry and also may improve the robustness, as it is hard for an intentional interference to attack multiple independent systems operating on different frequency bands. The performance improvement using multi-GNSS signals has been analyzed by many research groups since the availability of signals from GPS and GLONASS systems [7]. Joint GPS and GALILEO solution has been analyzed in terms of integrity improvement in [8]. Improvement in position solution using combined GPS and GLONASS system in the urban environment was demonstrated in [9]. The research work in [10] has shown the performance improvement using combined GPS and BeiDou signals compared to using only a single-system receiver. The Work in [11] proposed an analytical approach to assess the performance of all possible combinations of four GNSSs and shown that the performance of position solution is improved using the integration of two or more GNSSs. It was also shown in [11] that the performance improvement using three or more systems is less significant as compared to two GNSS system solution relative to a single system.

1.2 Motivation

Processing of GNSS signals from more than one frequency band enhances the accuracy and reliability of position solution in both standalone and differential positioning. To achieve this objective, modernized GNSS infrastructure is providing signals over multiple frequency channels to the civilian user. Now, the task of a GNSS receiver designer is to provide an answer to the following question,

"How to make use of multiple frequency channel signals in GNSS receivers to achieve high accuracy, availability, and reliability of position solution in time-varying GNSS signal environment?"

In a time-varying GNSS signal environment, signals from different frequencies are often subjected to dynamics and intentional or unintentional radio frequency interference. Processing of multiple frequency signals in such varying signal conditions is quite challenging to the receiver designer. Furthermore, receiver designer has to be aware of the characteristics of multiple frequency signals and the influence of various signal conditions on the performance of the receiver signal processing algorithms. Not one single algorithm or an approach may be suitable to process multiple frequency signals and to extract the performance benefits in all possible time-varying signal conditions.

In response to these challenges, the problem of multi-frequency GNSS signal processing has been pursued by many academic and industrial research groups, since the modernization of GNSS infrastructure with new civil signals. Motivated to be part of an ongoing research, this thesis aims to analyze the performance of multiple frequency signals and signal processing algorithms in challenging signal environment and it also aims to identify its limitations. Based on the insight of a prior performance analysis and to enable the mutual benefits of multi-frequency signals, this thesis develops novel collaborative and adaptive multi-frequency signal tracking algorithms in order to enhance the individual frequency signal tracking loop performance and subsequently to improve the position accuracy and reliability.

1.3 State-of-the-art research and limitations

In this section, state-of-the-art research work in GNSS multiple frequency signal processing is reviewed and also limitations of prior work are discussed.

1.3.1 Conventional multi-frequency signal processing

In conventional multi-frequency receiver, multiple signal code and carrier phase variations are tracked using independent Scalar Tracking Loop (STL). Then, weighted linear combination of observations are generated in the navigation processor to remove common-mode observation errors in order to improve the accuracy of position solution [12].

Limitation

A well-known limitation of conventional multi-frequency receiver in the generation of a linear combination of observations is the amplification of observation noise and multipath [12]. For instance, if the GPS L5/GALILEO E5 signal is combined with GPS L1/ GALILEO E1 signal in the observation domain, the overall multi-frequency receiver noise performance is degraded to that of GPS L1/ GALILEO E1 signal. The degradation occurs because, in challenging signal conditions, the L1 signal tracking loop observation noise is higher than that of L5 signal and this causes the amplification of combined signal observation noise. As a result, the performance of combined signal observation solution in weak signal conditions is determined by the signal of the lower C/N_0 tracking threshold.

1.3.2 Doppler-aided tracking algorithms

The Doppler-aided signal tracking is not a new concept in GNSS receiver. The carrier Doppler-aided code tracking loop is known to perform better than unaided carrier tracking loop in GNSS receiver [13] and its a well-known signal processing technique employed in every GNSS receiver. In a similar line, FLL-assisted Phase Locked Loop (F-PLL) in carrier phase tracking has better performance than PLL in challenging signal conditions [13]. Work in [14] and [15] has demonstrated improved GNSS signal tracking threshold performance under dynamic environment using external Doppler aiding from inertial measuring equipment in single-frequency receiver. In multi-frequency receiver, frequency diversity techniques such as inter-band Doppler-aided tracking is proposed in [16] for the L1/L5 signal combination. The performance of L2C Doppler-aided L1 carrier tracking to improve the resistance to RF interference is shown in [17]. Work in [18] presented the implementation of an adaptive inter-frequency aiding carrier tracking algorithm to enable improved tracking performances of the scintillating radio occultation signals. In inter-band Doppler-aided tracking, one of the multi-frequency signal tracking loop provides Doppler frequency information to co-existing frequency channel tracking loop, so that aided signal tracking loop bandwidth can be narrowed to track residual phase variations.

Limitation

Inter-band Doppler aiding allows the reduction of the loop bandwidth of the aided loop. The narrow loop bandwidth tracking improves the aided signal tracking loop noise performance. This process is beneficial under the assumption that the external noise induced from the Doppler aiding signal is relatively low. Otherwise, the propagation of noise through Doppler aid causes degradation of the aided signal tracking loop noise performance. Assumptions made in this approach are not unconditionally valid in changing

GNSS signal environment such as frequency selective interference. For instance, the lower frequency carrier L2C and L5 signal tracking is less robust to ionosphere scintillation than L1 signals [19]. Hence, L5 Doppler-aided L1 tracking proposed in [16] and L2C Doppler-aided L1 tracking in [17] tend to lose track in the ionosphere scintillation compared to conventional independent scalar tracking loop.

1.3.3 Vector tracking algorithms

The collaboration in multiple satellite signal tracking using space diversity techniques such as Vector Tracking Loop (VTL) is a well-known procedure followed in advanced GNSS receivers. In VTL, Doppler shift is estimated from velocity measurements in the navigation filter and provided as an aid to multiple satellite signal tracking channels. This process enhances the individual satellite signal tracking sensitivity in a weak signal environment by making use of the redundancy of satellite signals. The VTL was initially introduced in [20] for the DLL, and then the same concept was extended to the joint carrier tracking of multi-constellation satellite signals using Vector Phase Lock Loop (VPLL) in [21]. Different variants of the VTL architecture have been proposed by many research groups [22], [23], and the integrity of VTL techniques has been an active research topic in the past decade. A VPLL for joint tracking of multiple frequencies and multiple satellites was presented in [24] to improve the carrier tracking loop robustness by mapping tracking errors into position error, clock drift, ionospheric, and tropospheric errors.

Limitation

A well-known limitation of VTLs is the propagation of position errors in the navigation filter to all the tracking channels [25] and an inadequate update rate of the navigation filter. Despite these limitations, VTL architecture is widely employed in most of today's high-end GNSS receivers to improve the individual satellite signal tracking sensitivity in challenging signal environment such as an urban canyon.

1.3.4 Combined multi-frequency signal tracking algorithms

The frequency diversity of multiple frequency channels is utilized to enable combined multi-frequency channel tracking. A two-frequency signal tracking using combined discriminator output based Kalman filter tracking is proposed for GPS L1/L2C signals in [26] and the same concept was extended for GPS L1/L5 signals in [27] to enhance the individual signal tracking performance. Work in [28] showed tracking performance improvement in fading signal scenarios using combined correlator output based on two-frequency channel tracking approach. Recent research in [29] proposed a combined multi-frequency signal tracking using AKF to improve the tracking loop performance under ionospheric scintillation.

Limitation

The combined multi-frequency channel tracking performance is limited in the frequency selective interference condition, due to the propagation of measurement errors from a weak signal channel to stronger signal channels. Furthermore, combined multi-frequency channel tracking has neglected the residual phase and frequency differences between multiple frequency channels due to frequency dependent disturbances. The Kalman filter-based two-frequency signal tracking proposed in [26], [27] is a suitable solution in known signal environments under the assumption that the process noise and measurement noise statistics of each signal are known a prior. In practice, the assumed noise statistics

are not unconditionally valid for GNSS signal tracking in time-varying signal environments such as ionosphere scintillation, blockage, and interference. Hence, in the signal tracking KF, the process noise and measurement errors needs be estimated online from the signal measurements in order to adapt the Kalman gain in response to the changing signal level and dynamics.

1.4 Research objectives and contributions

The objective of this research thesis is to extract the performance benefits of multi-frequency GNSS signals in time-varying GNSS signal environments. To accomplish this objective, it is necessary to analyze the performance of each signal in varying signal conditions and to investigate suitable signal processing algorithms to enable optimum performance of multi-frequency GNSS signals.

The individual objectives of this thesis are summarized as follows:

- To analyze the performance achievable with GNSS signals from different frequencies.
- To find the optimum two-frequency signal combination for a standalone and differential positioning applications.
- To analyze the performance of conventional multi-frequency signal processing algorithms and limitations.
- To investigate the optimum dual-frequency signal processing algorithms for a robust and precise position using standalone dual-frequency receivers.
- To investigate the computationally efficient and robust multi-frequency channel tracking architecture to enhance individual frequency channel tracking threshold performance in all signal conditions.

To achieve these objectives, the major contributions made in this research thesis are summarized as follows:

- Currently, available GNSSs are transmitting signals over three to four carrier frequencies. However, not every signal or combination of signals is suitable to serve diversified requirements of civilian applications. The multiple frequency GNSS signal code and carrier frequencies are uniquely defined and transmitted at different RF spectrum. As a result, each of these signals has the different influence of channel effects. By considering the diversity in the performance of multiple signals, it is necessary to select a combination of frequencies leading to an optimum performance of existing civilian signals for an intended application. Hence, the performance of multi-frequency GNSS signals is analyzed using analytical error models. For an experimental verification, a multi-frequency GNSS software receiver is developed based on the open source single-frequency software receiver published by Prof. Kai Borre in [30], to analyze the performance of a combination of GPS L1, L2C, and L5 signals using live satellite data collected from block-IIF satellites [P1].
- Based on an insight of multiple frequency signal characteristics and performance limitations of scalar tracking loop architecture, the author investigated a suitable signal processing methods to enable the mutual benefit of multiple frequency signals.

The author also developed a common Doppler-aided two-frequency channel tracking loop software to analyze the performance benefits of collaboration in two-frequency signal tracking to enhance the receiver sensitivity, accuracy, and precision [P2].

- By making use of coherency in satellite signal generation, a computationally efficient centralized dynamics multi-frequency carrier tracking architecture is proposed to enhance the individual frequency channel tracking threshold performance. The multiple frequency signals transmitted from the same satellite are subject to both deterministic and non-deterministic disturbances while propagating through the atmosphere, which causes code and carrier phase variations in the received signal. Some of these changes are common across multiple frequency signals, while some are specific to each frequency channel. The common signal dynamics information in received multiple frequency signals can be estimated by means of a CTL, then, an effort to track them with individual frequency channel PLL can be reduced. This will enable the narrow bandwidth PLL tracking in each channel, and thus improve the individual signal tracking loop performance [P3].

- In real GNSS signal environment, multiple frequency signals from the same satellite often experience interference either at the same time or different time instants. The interference occurs in all the received frequency channels at the same time due to shadowed or blocked satellite in urban canyon or foliage. The interference occurs on selected frequency channels at different time instants due to multipath or intentional meaconing/jamming/spoofing. To improve tracking loop performance in such challenging signal environments, it is necessary to sense the signal condition in each frequency channel for co-operative multi-frequency channel tracking. This was realized by making use an adaptive Kalman filter in CTL to enable adaptive tracking loop bandwidth in response to the changing signal power levels and dynamics.

- The performance benefits of proposed centralized dynamics multi-frequency carrier tracking architecture were analyzed in comparison to the scalar tracking loop architecture. For experimental verification, an adaptive multi-frequency signal tracking loop software is developed and the robustness of the proposed approach was tested by subjecting to the matched spectrum jamming waveform in [P5].

1.5 Author's contributions

The author of this thesis is the main contributor to publications [P1]-[P5]. None of the publications has been used or is planned to be used as a part of another thesis. The author acquired the consent of the co-authors to use these publications as a part of this thesis.

- In [P1], the author proposed the concept of the research work based on discussions with the second author. The author carried out theoretical analysis and developed a multi-frequency GNSS software receiver for experimental validation of the proposed concept. The author wrote more than 80 % of the manuscript.

- In [P2], the author proposed the dual-frequency signal processing architecture and received feedback from the second author. The author made all the theoretical analysis and carried out the full experimental validation. The author wrote the full manuscript. The second author contributed in giving feedback, providing minor corrections on the architecture, and reviewing the manuscript.

- In [P3], the author proposed the concept of joint tracking of multi-frequency signals and had discussions with co-authors for theoretical validation. The author developed a software for experimental validation and wrote the manuscript. The manuscript was reviewed by the co-authors.
- In [P4], the author proposed the concept and made a theoretical analysis. The author also developed a software to verify the theoretical analysis and wrote the manuscript. The second author contributed with feedback and reviews of the manuscript.
- In [P5], the author proposed the concept of multi-frequency signal dynamics tracking using AKF and further discussed with the co-authors for technical validation and improvements of the tracker. The author made the theoretical analysis and developed a software for experimental verification of the proposed concept. The author wrote more than 80 % of the manuscript. The manuscript was reviewed by the co-authors.

1.6 Outline of thesis

The contributions of this research work are presented in the following chapters. The outline of the rest of the thesis organization is detailed below.

Chapter 2 presents a review of multiple frequency signal characteristics of four GNSS and two RNSS. The characterization of multiple frequency channel phase variations due to propagation effects is analyzed. A brief description of conventional multi-frequency signal processing architecture and standard tracking algorithms are presented. The tracking loop design criteria are reviewed from the literature. Subsequently, the generation of linear combination of multi-frequency signal observations and navigation solution is discussed.

Chapter 3, defines the key parameters to analyze the performance of multi-frequency GNSS signals. The performance analysis of linear combination of observations in multi-frequency receiver is discussed. The criteria to find optimum two-frequency signals for a standalone ionosphere-free solution and wide-lane integer ambiguity solution of carrier phase observations in differential positioning applications is presented.

The conventional dual-frequency receiver generates the weighted linear combination of observations to remove ionosphere delay error. This process is limited by the amplification of noise and less performance signal. To overcome this limitation, common Doppler estimate based two-frequency signal tracking followed by carrier Doppler smoothing is proposed, which is briefly discussed in Chapter 4. The performance benefits of the proposed architecture are shown using live satellite data collected over GPS L1 and L5 frequencies from block-IIF satellites.

To overcome the performance limitations of scalar multi-frequency channel tracking loop, it necessary to sense the signal environment to design an optimum signal tracking loops. This has lead to the proposed centralized dynamics multi-frequency channel tracking using adaptive Kalman filter presented in Chapter 5. Furthermore, an approach to use multiple frequency channel measurements to estimate common signal dynamics is defined in time-varying signal conditions to avoid the propagation of weak channel measurement errors to stronger channels.

The performance of the proposed centralized dynamics multi-frequency carrier tracking architecture is analyzed in comparison to fixed bandwidth tracking loops. The performance benefits of adaptive signal tracking algorithms are discussed in Chapter 6.

Finally, the conclusion about the contributions of this research and findings are presented. Based on the assumptions, limitations, and issues experienced in this research thesis, the scope of future work is proposed.

2 Multi-frequency GNSS Signals

This chapter gives an introduction to multi-frequency GNSS signals and signal processing in GNSS receiver. It starts with an overview of the main characteristics of four existing GNSS and two existing RNSS civil signals. Subsequently, the objectives of multi-frequency GNSS signal transmission are discussed in brief. Then, the details of multi-frequency signal processing in GNSS receiver are given.

The main contributions of this chapter consist of:

- Review of the GNSS and RNSS multi-frequency civil signal characteristics, their performance metrics, and requirements.
- Characterization of the received multi-frequency GNSS signal-phase variations.
- Review of the standard multi-frequency GNSS signal processing architecture and the performance bounds on multiple frequency signal tracking loops.
- Discussion on the optimum scalar tracking loop design criteria.
- Discussion of the process of generating the linear combination of multi-frequency signal observations and computation of position solution.

2.1 Introduction

A brief review of multi-frequency civil signal characteristics of four GNSS [31], [32], [33], [34] and two RNSS [35], [36] is given in table 2.1 for relative comparison. A detailed description of the significance of each modulation enumerated in table 2.1 can be found in [11].

The objective of multi-frequency GNSS signal transmission is to enable the GNSS receiver to overcome the inherent limitations of accuracy and reliability in single-frequency solution. To accomplish this objective, the GNSS multiple frequency signals are designed with unique signal characteristics, suitable for a wide range of civilian applications and allocated to separate RF spectra in the L-band as shown in a table 2.1. Some of these signals are transmitting at higher power levels and higher chip rates to enable high signal tracking sensitivity and an improved signal observation precision [37]. New civil signals are transmitted as a composite of dual-channel: data and pilot. The data channel carries the navigation data, while the pilot channel is data-less. Data-less channel tracking has an advantage of longer signal integration time in high-sensitivity applications [38]. Although each of the multiple frequency signals has one or more key advantages, no single signal will be best suited for every case. Hence, each combination of these signals can

Table 2.1: GNSS and RNSS multi-frequency signal characteristics

Signal type	Frequency (MHz)	Min. power (dBW)	Modulation	Channel type	Chip rate (Hz)
GPS L1 C/A	1575.42	-158.5	BPSK(1)	Data	1.023
GPS L1C	1575.42	-157	BPSK(1)	Data, Pilot	1.023
GPS L2C	1227.6	-160	BPSK(1)	Data, Pilot	1.023
GPS L5	1176.45	-157	QPSK(10)	Data, Pilot	10.23
GLONASS L1	1598.0625 - 1605.375	-161	BPSK(0.511)	Data	0.511
GLONASS L2	1242.937 - 1248.625	-167	BPSK(0.511)	Data	0.511
GLONASS L3	1201	-167	BPSK(4)	Data, Pilot	4.092
GALILEO E1	1572.42	-160	CBOC	Data, Pilot	1.023
GALILEO E6	1278.75	-155	BPSK(5)	Data, Pilot	5.115
GALILEO E5	1191.795	-155	AltBOC(15,10)	Data, Pilot	10.23
BeiDou B1	1561.098	-163	QPSK(2)	Data	2.046
BeiDou B2	1207.14	-163	QPSK	Data	2.046
BeiDou B3	1268.52	-163	QPSK(10)	Data	10.23
NavIC L5	1176.45	-159.8	BPSK	Data	1.023
NavIC S1	2492.08	-163.1	BPSK	Data	1.023
QZSS L1 C/A	1575.42	-158.5	BPSK	Data	1.023
QZSS L1C	1575.42	-157	BOC(1,1)	Data, Pilot	1.023
QZSS L2C	1227.6	-160	BPSK	Data, Pilot	1.023
QZSS L5	1176.45	-157.9	BPSK(10)	Data, Pilot	10.23

be used to serve different civilian applications. For example, in GPS system, L1 signal at higher carrier frequency has the lowest ionosphere refraction error, L5 signal has the highest transmission power and code rate and is also transmitted in Aeronautical Radio Navigation Service (ARNS) band, and L2C signal with long code length has the best cross-correlation performance [39].

The multi-frequency GNSS signal scenario is shown in Fig. 2.1. Each of the received multi-frequency signals provide range and range rate information between the satellite and user receiver. However, these signals transmitted over different RF channels tend to have different channel effects. As a result, the accuracy and precision of range and range-rate observations at each frequency channel vary significantly. The frequency diversity of multiple civilian frequency signals can be utilized to generate linear combinations of two or more signal code and carrier-phase observations in order to eliminate common-mode errors incurred in the signal propagation path to improve the observation accuracy.

In low-to-medium accuracy applications (i.e., accuracy range of 10 m – 30 m), a single-frequency solution is sufficient. For high-accuracy applications (i.e., accuracy range of 10 cm – 1 m), two-frequency signals are often used for different purposes such as ionosphere-delay-free (ionosphere-free) combination, wide-lane combination in carrier-phase integer ambiguity resolution and narrow-lane combination in order to generate a low-noise signal observations in fixed-integer mode [40]. For instance, the ionosphere-free combination is used in both standalone high accuracy positioning and in differential carrier-phase positioning to extend base-line length [41]. The wide-lane combination of carrier-phase observations increases the wavelength, which will lead to the faster convergence of integer ambiguity resolution. The narrow-lane combination reduces the observation noise, which in turn improves the precision in position solution. Furthermore, the precise carrier-phase positioning applications (i.e., accuracy in the order of mm) also benefit from a third frequency to eliminate higher order ionosphere delay error [42] and to facilitate the ambiguity resolution through techniques known as Three Carrier Ambiguity

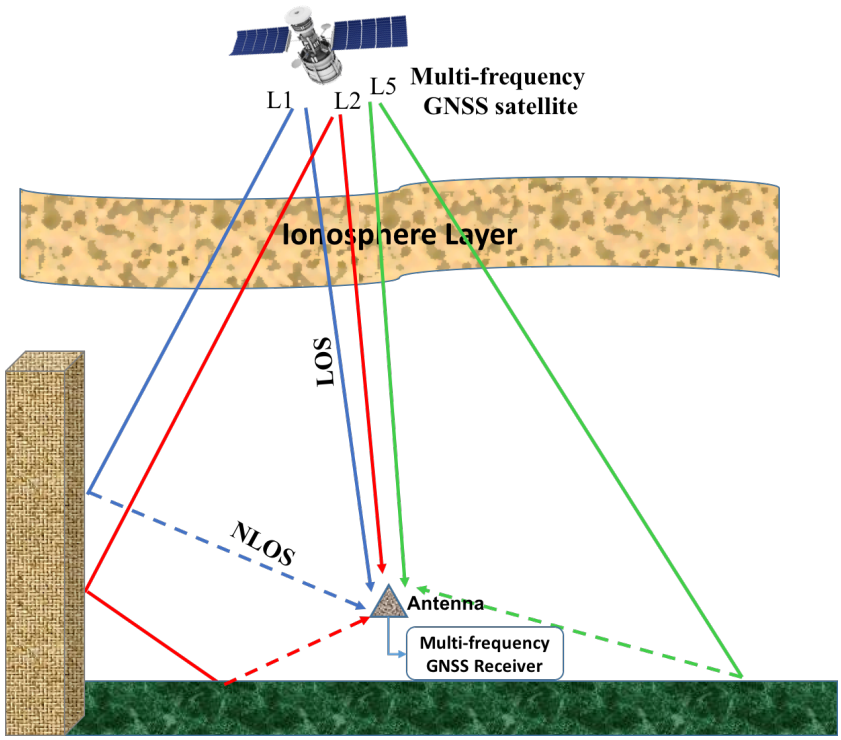

Figure 2.1: Multi-frequency GNSS signal scenario

Resolution (TCAR) [43], [44], [45]. For the safety-of-life applications, the reliability and continuity of service can be achieved through redundancy of multiple frequency signals [P3].

The ionosphere delay estimation using the difference between the two frequency signal range observations is more accurate when the difference between the two carrier frequencies is larger [12]. The carrier-phase integer ambiguity estimation needs wide-lanes with large wavelength to attain high success rate and faster convergence [46]. The wide-lane with large wavelength can be generated using closely spaced signals in the RF spectrum. It is to be noticed that the requirement of two-frequency signals for ionosphere delay estimation is opposite to that of carrier-phase ambiguity estimation. To meet the diversified frequency requirements of civilian applications, most of the GNSS systems are transmitting on three to four civil signal frequencies. In choosing between single or combination of multiple frequency signals, a receiver designer has to look at the best trade-off between the intended application requirements and the complexity of user equipment such as [40],

- Availability: is the percentage of time the navigation or timing solution can be computed by the user. These values vary typically in the range of 95 - 99.95 %.
- Accuracy: is the difference between the computed position and the true position. Typical values of the position accuracy range from tens of meters to centimeters. Accuracy is stated in terms of horizontal and vertical position accuracy in navigation receivers and time accuracy in timing receivers.

- Continuity: is the ability to provide the required performance during the operation without failure in service. A typical value is $1\text{x}10^{-4}$ over the course of the procedure where the system is in use.
- Sensitivity: is the minimum carrier-to-noise ratio of the received GNSS signal, above which the signal tracking loop error is below the acceptable error threshold. Typical values of GNSS receiver sensitivity range from -160 dBm to -125 dBm.
- Robustness: is the ability to withstand or mitigate the intentional or unintentional interference.
- Power consumption: is the amount of power a device uses to provide a position information. The power consumption of the positioning technology will vary depending on the available signals.
- Size of the receiver: is influenced by several factors, such as antenna design, the complexity of the receiver hardware and software.
- Cost of the receiver: is also influenced by several factors, such as receiver capabilities and ruggedness.

Hence, it is necessary to select the combination of multiple frequency signals leading to an optimum performance for an intended application using a thorough analysis as it will be discussed in the next chapter. The scope of the research work presented in this thesis is limited to the baseband signal processing stage of the multi-frequency GNSS receiver.

2.2 Characterization of multi-frequency GNSS signals

The multi-frequency GNSS signals incident on the receiver's antenna can be represented as a composite sum of individual frequency signals plus noise at the specified frequency band k,

$$s(t) = \sum_{k=1}^{N} \left(\sqrt{P_k} C_k(t-\tau_k) D_k(t-\tau_k) e^{j(2\pi f_{L_k}(t)t + \phi_k(t))} + n_k(t) \right), \tag{2.1}$$

where P_k is the received signal power; $C_k(t)$ is the pseudo-random code; $D_k(t)$ is the navigation message data bits; τ_k is the transition delay from satellite to the receiver; $f_{L_k}(t)$ is the signal carrier frequency and $\phi_k(t)$ is the signal carrier-phase; finally, $n_k(t)$ is the noise in the k-th frequency channel. The received signal carrier-phase $\phi_k(t)$ represents the signal phase dynamics, including satellite-induced Doppler, Doppler drift and user-dynamics-induced phase variations. The received signal carrier-phase can be represented using Taylor's approximation as,

$$\phi_k(t) = \phi_k(t_0) + (t-t_0)\dot{\phi}_k(t_0) + \frac{(t-t_0)^2}{2}\ddot{\phi}_k(t_0) + \varepsilon_{\phi_k}, \tag{2.2}$$

where $\phi_k(t_0)$, $\dot{\phi}_k(t_0)$ and $\ddot{\phi}_k(t_0)$ are the received signal phase and its time derivatives at time t_0, in cycles, cycles/s and cycles/s^2 respectively; ε_{ϕ_k} is the error in the approximation. The rate of change of phase is simply the Doppler frequency of the signal, hence, Eq. 2.2 can be written as,

$$\phi_k(t) = \phi_k(t_0) + (t-t_0) f_{D_k}(t_0) + \frac{(t-t_0)^2}{2}\dot{f}_{D_k}(t_0) + \varepsilon_{\phi_k}, \tag{2.3}$$

where $f_{D_k}(t_0)$ and $\dot{f}_{D_k}(t_0)$ are the Doppler frequency and the rate of Doppler frequency of k-th carrier frequency in cycles/s and cycles/s^2, respectively.

The received multi-frequency GNSS signal code and carrier-phase variations are subjected to deterministic and non-deterministic disturbances due to many error sources in the propagation channel. Some of these disturbances are common across multiple frequency signals, while some are specific to each frequency channel. The common phase variations are due to LOS relative movement between the satellite and receiver. The channel specific phase variations are due to frequency dependent error sources such as ionosphere Total Electron Content (TEC) variations and receiver reference clock frequency drift.

The geometric Doppler shift depends on the relative movement between the satellite and receiver, while the ionospheric Doppler shift depends on the signal propagation path through the atmosphere [4]. The Doppler shift due to reference clock frequency drift is introduced through down conversion and sampling process at the RF front-end [14]. Finally, the received satellite signal carrier frequency deviation at k-th frequency channel can be represented as a combination of geometric Doppler shift f_{GD_k} and residual Doppler shift f_{RD_k}, due to ionospheric Doppler shift f_{ID_k}, and reference clock Doppler shift f_{CD_k},

$$\begin{aligned} f_{D_k} &= f_{GD_k} + f_{RD_k} \\ f_{RD_k} &= f_{ID_k} + f_{CD_k}. \end{aligned} \tag{2.4}$$

2.2.1 LOS - dynamics

The geometric Doppler shift, f_{GD_k} can be expressed as the velocity of the receiver relative to the transmitter in the LOS direction, scaled by the carrier wavelength. This relation can be expressed as,

$$\begin{aligned} f_{GD_k} &= \frac{1}{\lambda_k} \left(\mathbf{v}_R - \mathbf{v}_S\right) . \overrightarrow{\mathbf{1}}_{LOS}, \\ \lambda_k f_{GD_k} &= \left(\mathbf{v}_R - \mathbf{v}_S\right) . \overrightarrow{\mathbf{1}}_{LOS} = \delta\dot{\rho}, \end{aligned} \tag{2.5}$$

where λ_k is the wavelength of the carrier signal at subscripted frequency channel; $\mathbf{v}_R$ and $\mathbf{v}_S$ are receiver and satellite velocities in the LOS direction, respectively; $\overrightarrow{\mathbf{1}}_{LOS}$ is the unit LOS vector from receiver to satellite; $\delta\dot{\rho}$ is the LOS range rate between satellite and receiver; typical range of LOS Doppler frequency is -5 kHz to +5 kHz for static receiver and -10 kHz to +10 kHz for dynamic receiver.

2.2.2 Ionosphere TEC - dynamics

The changing TEC in the ionosphere layer results in a Doppler shift f_{ID_k} in the received satellite signal, which is relatively small compared to the LOS geometric Doppler shift, and can be computed as [4],

$$f_{ID_k} = \frac{1.34 \times 10^{-7}}{f_{L_k}} \left(\frac{\partial(TEC)}{\partial t}\right). \tag{2.6}$$

As shown in [4], an upper limit to the rate of change of TEC to the stationary user is approximately $0.1 \times 10^{16} \left(\frac{el}{m^2}/s\right)$, which in turn results in an additional frequency shift of 0.085/0.1/0.1 Hz at L1/L2/L5 frequencies. From Eq. 2.6, we can see that the ionospheric Doppler shift is a frequency dependent error.

2.2.3 Reference oscillator - dynamics

The reference oscillator in the receiver is sensitive to the platform dynamics, such as acceleration and jerk. This causes the oscillator frequency to drift over time, which in turn results in an additional apparent Doppler shift in the down converted received signal. The drift in the reference oscillator frequency subject to the acceleration dynamics is [14],

$$\Delta f_{ref} = s_g f_{ref} a_g, \tag{2.7}$$

where a_g is the acceleration in units of g, $g = 9.8$ m/s^2; f_{ref} is the reference clock frequency; s_g the reference oscillator sensitivity to the acceleration, which varies with the type of reference oscillator. Typical values of acceleration sensitivity are, $s_g = 5 \times 10^{-9}/g$ for a TCXO, or $s_g = 3.5 \times 10^{-9}/g$ for an OCXO. The drift in the reference clock frequency propagates as a Doppler shift in the reference carrier signal f_{L_k}, which can be expressed as,

$$f_{CD_k} = s_g f_{L_k} a_g. \tag{2.8}$$

For instance, at an acceleration of $a_g = 1g$, the Doppler shift in L1/L2/L5 reference clock frequency generation is about 7.8/6.2/5.8 Hz using a TCXO and 5.5/4.2/4.1 Hz using an OCXO. From Eq. 2.8, it is inferred that the influence of reference oscillator Doppler shift also depends on the received signal frequency.

2.2.4 Coherency in satellite signal generation

Typically, the code and carrier frequencies of multiple frequency signals from the same satellite are synchronously generated from a common reference clock. For instance, GPS L1, L2C, and L5 signals are generated synchronously from the reference clock frequency, $f_{ref} = 10.23$ MHz. Hence, the three signal code and carrier frequencies are linearly related to f_{ref} as,

$$\begin{aligned} &f_{L_k} = \alpha_k f_{ref} \ ; \ f_{cL_k} = \beta_k f_{ref} \ ; \ k = \{1, 2, 5\} \\ &\alpha_1 = 154, \quad \alpha_2 = 120, \quad \alpha_5 = 115, \\ &\beta_1 = \beta_2 = 1/10, \quad \beta_5 = 1, \end{aligned} \tag{2.9}$$

where f_{L_k} and f_{cL_k} are the carrier and code frequencies of subscripted GPS L-band signals.

From Eq. 2.9, the LOS geometric Doppler shift in the code and carrier frequencies of three GPS civil signals is linearly related as,

$$\begin{aligned} &\lambda_{L_1} f_{GDL_1} = \lambda_{L_2} f_{GDL_2} = \lambda_{L_5} f_{GDL_5} = \delta\dot{\rho}, \\ &\lambda_{cL_1} f_{cdL_1} = \lambda_{cL_2} f_{cdL_2} = \lambda_{cL_5} f_{cdL_5} = \delta\dot{\rho}, \end{aligned} \tag{2.10}$$

where λ_{cL_k} and λ_{L_k} are the wavelength of the code and carrier frequency; f_{cdL_k} and f_{GDL_k} are the geometric Doppler shift in the code and carrier frequency of the subscripted frequency channel. From Eq. 2.10, it is inferred that the geometric Doppler shift in each frequency channel can be obtained from the Doppler shift or range rate of the co-existing frequency channel with appropriate scaling with the wavelength of the received signal carrier frequency.

The LOS geometric Doppler shift is significantly higher than the residual Doppler shift due to ionosphere TEC changes and drift in the reference clock frequency. The LOS

Doppler shift component can be estimated in several ways, either by taking measurements from co-existing frequency channels or co-existing satellite signals or external aiding from inertial sensors. The residual Doppler shift due to frequency dependent error sources can be estimated only by the specific channel-phase measurements.

2.3 Multi-frequency GNSS receiver architecture

A wide-band RF front-end and a multi-channel digital signal processing unit are required to process signals from multiple RF frequency bands. The RF front-end receives signals incident on the antenna and downconverts them to an Intermediate Frequency (IF) or to baseband. The down-converted signal is subsequently sampled and quantized to produce digital complex in-phase (I) and quadrature-phase (Q) signal. The digitized complex baseband data will be further processed in a digital signal processing module in three stages: *acquisition, tracking, and navigation blocks*. The acquisition is a one time process, that coarsely estimates the code-phase and carrier Doppler frequency of visible satellite's signal. Signal tracking continuously tracks the signal code and carrier-phase variations with fine resolution using code and carrier tracking loops. The tracking process also demodulates the satellite navigation data [12]. Finally, those data along with timing information are passed to the navigation block which extracts ephemerides from navigation data and computes position solution using the ionosphere-free linear combination of pseudorange observations of multiple frequency signals from four or more satellites. The functional diagram of a classical multi-frequency GNSS receiver signal processing architecture is shown in Fig. 2.2.

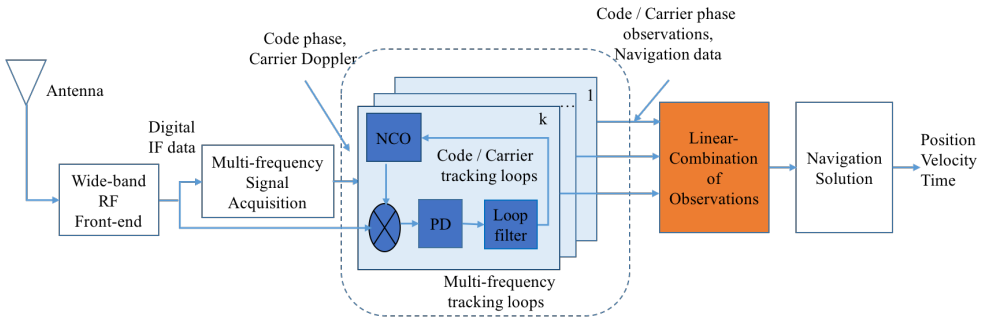

Figure 2.2: Classical multi-frequency GNSS receiver architecture

2.4 Multi-frequency signal acquisition

In multi-frequency GNSS receiver, multiple signal acquisition can be done in different ways by considering the fact that the code and carrier frequencies are coherently related on these signals for a given GNSS satellite. One way is to simultaneously perform the acquisition process on each frequency channel to obtain code-phase, τ, and Doppler frequency, f_d, parameters of visible satellites. Another way is to acquire signals at one frequency, and these acquisition parameters (f_d, τ) can be scaled and used interchangeably to acquire signals at other frequency as discussed in [47], [38]. Finally, the coarse values of the code-phase and Doppler frequency of multiple carrier signals from visible satellites will be forwarded to multi-frequency tracking loop architecture, which is discussed in the following section.

2.5 Standard multi-frequency tracking loop architecture

A conventional multi-frequency GNSS receiver signal tracking stage has multiple individual signal code and carrier tracking channels. Each one tracks a single-frequency signal received from the satellite. Fig. 2.3 illustrates the standard code and carrier tracking loop architecture for multiple frequency channels. The code/carrier-phase tracking loop is implemented in a feedback control loop which tracks the received signal code/carrier-phase using estimates of the code/carrier-phase error between the received and reference signal. The code/carrier-phase tracking loop in each frequency channel is build up with a complex correlator (Mixer, Integrator and Dump (I & D)), code/carrier Phase Discriminator (PD), code/carrier-phase loop filter and code/carrier Numerically Controlled Oscillator (NCO). Each tracking channel synchronizes the receiver reference signal code and carrier frequency with that of the received satellite signal, by controlling the reference signal code and carrier frequency generator.

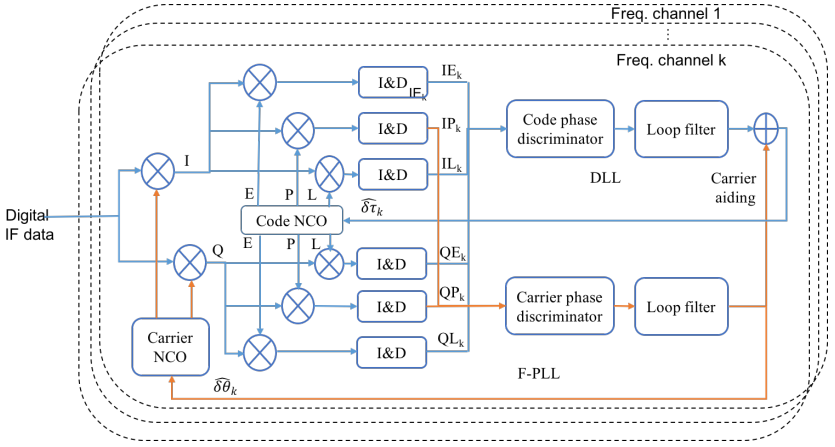

Figure 2.3: Standard multi-frequency GNSS signal tracking architecture

The estimation of code and carrier-phase error in code-carrier tracking loop is obtained by correlating the received signal with the local reference carrier signal. The resultant baseband signal early, prompt, and late code correlator output have two components in each channel at specified frequency band k: In-Phase and Quadrature-Phase, i.e. IE_k, QE_k, IP_k, QP_k, IL_k, QL_k.

$$
\begin{aligned}
IE_k &= A_k(t)C_k(t)D_k(t)R(\delta\tau_k(t) - d)\cos(\delta\theta_k(t)) + n_{IE_k}(t) \\
QE_k &= A_k(t)C_k(t)D_k(t)R(\delta\tau_k(t) - d)\sin(\delta\theta_k(t)) + n_{QE_k}(t) \\
IP_k &= A_k(t)C_k(t)D_k(t)R(\delta\tau_k(t))\cos(\delta\theta_k(t)) + n_{IP_k}(t) \\
QP_k &= A_k(t)C_k(t)D_k(t)R(\delta\tau_k(t))\sin(\delta\theta_k(t)) + n_{QP_k}(t) \\
IL_k &= A_k(t)C_k(t)D_k(t)R(\delta\tau_k(t) + d)\cos(\delta\theta_k(t)) + n_{IL_k}(t) \\
QL_k &= A_k(t)C_k(t)D_k(t)R(\delta\tau_k(t) + d)\sin(\delta\theta_k(t)) + n_{QL_k}(t) \\
A_k(t) &= \frac{\sqrt{P_k}}{2}\sin\left(\frac{\pi\delta f_k(t)T}{\pi\delta f_k(t)T}\right)
\end{aligned}
\tag{2.11}
$$

where R is the correlator output; d is the correlator chip spacing; T is the signal Pre-detection Integration Time (PIT); $\delta\tau_k(t)$, $\delta\theta_k(t)$ and $\delta f_k(t)$ are the mean values code-phase error, carrier-phase and frequency errors, respectively in subscripted frequency channel, $n_X(t)$ is the noise in the subscripted correlator output. The six correlator outputs shown in Eq. 2.11 are used to measure the code/carrier-phase and frequency error between the received signal and reference signal, using the code/carrier-phase and frequency discriminators.

The code-phase error can be measured either using coherent Delay Lock Loop (DLL) discriminator or non-coherent DLL discriminator. The coherent DLL is used when the carrier-phase is known i.e. $\delta\theta_k(t) = 0$. To avoid dependence on the carrier-phase, non-coherent DLL is preferred in most of the GNSS receivers [12]. From the complex early and late correlator outputs shown in Eq. 2.11, the code-phase error in non-coherent DLL loop can be measured using normalised early-late envelope discriminator [48]. The code-phase error measurement is non-linear, that is approximately equal to the actual code-phase error plus measurement noise,

$$\begin{aligned} e_{\tau_k} &= \delta\tau_k(t) + n_{\tau_k}, \\ \delta\tau_k(t) &= (1 - d/2)\,\frac{\sqrt{IE_k^2 + QE_k^2} - \sqrt{IL_k^2 + QL_k^2}}{\sqrt{IE_k^2 + QE_k^2} + \sqrt{IL_k^2 + QL_k^2}} \end{aligned} \tag{2.12}$$

where n_{τ_k} is the code-phase measurement noise in k-th frequency channel.

The carrier-phase error measured using non-linear phase discriminator, is approximately equal to the actual carrier-phase error plus measurement noise,

$$e_{\phi_k} = \delta\phi_k(t) + n_{\phi_k} \tag{2.13}$$

where n_{ϕ_k} is the non-linear phase discriminator measurement noise.

In the case of dual-channel tracking, the pilot channel phase error is measured using four-quadrant arc-tangent discriminator in conventional PLL loop. The data channel phase error is measured using two-quadrant arc-tangent discriminator in Costas PLL as given in Eq. 2.14, because the Costas-loop is insensitive to the data bit transition.

$$\begin{aligned} \delta\phi_k(t) &= \tan^{-1}\left(\frac{QP_k}{IP_k}\right) \text{ (Data channel)}, \\ \delta\phi_k(t) &= ATAN2\,(QP_k, IP_k) \text{ (Pilot channel)} \end{aligned} \tag{2.14}$$

The frequency error in the Frequency Lock Loop (FLL), measured using four-quadrant arc-tangent discriminator over the measurement interval, $(t_2 - t_1)$, can be expressed as,

$$\begin{aligned} e_{f_k} &= \delta f_k(t) + n_{f_k}, \\ \delta f_k(t) &= \frac{ATAN2\,(dot, cross)}{t_2 - t_1} \\ dot &= IP_k(t_1)IP_k(t_2) + QP_k(t_1)QP_k(t_2) \\ cross &= IP_k(t_1)QP_k(t_2) - IP_k(t_2)QP_k(t_1) \end{aligned} \tag{2.15}$$

where n_{f_k} is the non-linear frequency error measurement noise.

The code/carrier-phase and frequency error measurements in code/carrier-phase tracking loops are corrupted by two dominant error sources: thermal noise error and steady-state dynamic tracking errors. Hence, the code/carrier-phase error measurements will be further processed by the code/carrier-phase tracking loop filters to eliminate non-linear discriminator measurement noise and to estimate the true code/carrier-phase and frequency difference between the received and reference signals.

2.5.1 Dual-channel signal tracking approach

The new civil GNSS signals (Eg. GPS L2C/L5 and GALILEO E1/E2/E5) are designed as a composite of dual-channel: data and pilot. These dual-channel signals can be processed as either single-channel or dual-channel. Significant research has been carried out in evaluating the performance of single and dual-channel processing, more detailed information can be found in [38], [49]. To benefit from the total incoming power, the receiver needs to process both the pilot and data channel, with separate correlators and discriminators, and then to combine the results appropriately. This approach is computationally expensive. There are different strategies for dual-channel tracking, where the correlators are combined and a single discriminator is used to compute the phase error. However, coherent integration time in dual-channel (data+pilot) tracking is limited to navigation bit period due to unknown bit transition in the data channel. In the case of single-channel tracking, it is advantageous to process the pilot channel and to use the code and carrier-phase observations to demodulate the navigation message from the data channel. Although each signal component has only half the total power, processing pilot channel using a PLL with 6 dB advantage in tracking threshold gives an overall gain of 3 dB, see [16].

2.5.2 Tracking loop design criteria

The signal tracking loop design is characterized by the pre-detection integrator, loop discriminator, and the loop filter. These three functions determine the signal tracking loop noise performance and dynamic response. A rule-of-thumb design criterion for tracking loop threshold in DLL/PLL/FLL is that the 3-sigma value of the jitter due to all the sources of loop errors must not exceed the linear range of the DLL/PLL/FLL discriminators. This can be expressed in terms 1-sigma error tracking threshold criteria as [48],

$$\begin{aligned}
\sigma_{\delta\tau} &= \sigma_{\tau_{dll}} + \frac{\tau_e}{3} \leq \frac{d}{3} \ \text{[chips] DLL} \\
\sigma_{\delta\phi} &= \sigma_{\tau_{pll}} + \frac{\phi_e}{3} \leq 0.26 \ \text{[cycles] Costas-PLL} \\
\sigma_{\delta\phi} &= \sigma_{\tau_{pll}} + \frac{\phi_e}{3} \leq 0.52 \ \text{[cycles] PLL} \\
\sigma_{\delta f} &= \sigma_{\tau_{fll}} + \frac{f_e}{3} \leq \frac{1}{12T} \ \text{[Hz] FLL}
\end{aligned} \tag{2.16}$$

Where $\sigma_{\tau_{dll}}$, $\sigma_{\tau_{pll}}$, $\sigma_{\tau_{fll}}$ are thermal noise jitter in DLL, PLL, and FLL respectively; τ_e, ϕ_e, f_e are steady state dynamic tracking errors in DLL, PLL, and FLL respectively. The

performance of code and carrier-phase tracking loop is assessed by the 1-sigma value of total error due to all the sources.

It is to be noted that, the data-less channel tracking using PLL loop with longer integration time reduces the squaring loss, and thus lowers the tracking threshold up to 6-dB. Hence, the pilot channel tracking of modern GNSS signals has benefit of high signal tracking sensitivity compared to signals tracked using data channels [37], [49].

2.5.3 Thermal-noise error

The 1-sigma value of thermal noise jitter in DLL, PLL, and FLL can be expressed as a function of the code and carrier tracking loop bandwidths, pre-detection integration time, T, and carrier-to-noise spectral density ratio, c/n_0 ($= 10^{0.1C/N_0}$ for C/N_0 in dB-Hz),

$$\begin{aligned}
\sigma_{\tau_{dll}} &= \left(\frac{d}{2\pi}\right)\sqrt{\frac{B_{dll}\left(1+\frac{1}{2Tc/n_0}\right)}{c/n_0}} \quad \text{[chips]} \\
\sigma_{\tau_{pll}} &= \left(\frac{1}{2\pi}\right)\sqrt{\frac{B_{pll}\left(1+\frac{1}{2Tc/n_0}\right)}{c/n_0}} \quad \text{[cycles]} \\
\sigma_{\tau_{fll}} &= \left(\frac{1}{2\pi T}\right)\sqrt{\frac{4B_{fll}\left(1+\frac{1}{Tc/n_0}\right)}{c/n_0}} \quad \text{[Hz]}
\end{aligned} \tag{2.17}$$

Where B_{dll}, B_{pll} and B_{fll} are the loop bandwidths of the DLL, PLL, and FLL tracking loops, respectively.

Here, the oscillator jitter effects are neglected based on the assumption that the reference oscillator has good short-term phase stability characteristics.

2.5.4 Dynamic stress error

The dynamic stress error characterizes the transient response of the tracking loop to input signal dynamics such as acceleration and jerk in the carrier-phase. The dynamic stress in the receiver tracking loop is induced due to multiple sources such as LOS signal dynamics, ionosphere TEC variations and receiver reference oscillator sensitivity to platform dynamics. The dynamic stress error due to LOS signal dynamics is significantly higher than that of other sources. The loop order is sensitive to the same order of dynamics (first order to velocity stress, second order to acceleration stress, and third order to jerk stress), and the loop bandwidth must be wide enough to accommodate these higher-order dynamics. In carrier-aided code tracking loop, dynamic stress error (τ_e) is negligible and a code tracking loop can employ narrow bandwidth filter to obtain high precision. Also, the dynamic stress error in carrier tracking loop can be reduced with external Doppler aiding from inertial devices under dynamic environment.

2.5.4.1 LOS - dynamic stress error

The LOS dynamic stress error (ϕ_e) in the first, second, and third-order PLL can be determined from the following steady-state errors [48],

$$\begin{aligned}
\phi_e &= 0.25\frac{\delta\dot{\phi}}{B_{pll}} \text{ [cycles], for velocity dynamic error in first-order PLL} \\
\phi_e &= 0.2809\frac{\delta\ddot{\phi}}{B_{pll}^2} \text{ [cycles], for acceleration dynamic error in second-order PLL} \\
\phi_e &= 0.4828\frac{\delta\dddot{\phi}}{B_{pll}^3} \text{ [cycles], for jerk dynamic error in third-order PLL}
\end{aligned} \tag{2.18}$$

Similarly, the LOS dynamic stress error in the first and second-order FLL can be determined from the following steady-state errors,

$$\begin{aligned}
f_e &= 0.2809\frac{\delta\dot{f}}{B_{fll}} \text{ [Hz], for acceleration dynamic error in first-order FLL} \\
f_e &= 0.4828\frac{\delta\ddot{f}}{B_{fll}^2} \text{ [Hz], for jerk dynamic error in second-order FLL,}
\end{aligned} \tag{2.19}$$

where $\delta\dot{\phi}$, $\delta\ddot{\phi}$ and $\delta\dddot{\phi}$ are first, second and third-order phase error variations due to maximum LOS velocity, acceleration and jerk signal dynamics, cycles/s, cycles/s^2, cycles/s^3 respectively; $\delta\dot{f}$ and $\delta\ddot{f}$ are the maximum LOS acceleration and jerk signal dynamics, cycles/s^2 and cycles/s^3, respectively.

2.6 Optimum scalar tracking loop design criteria

The signal tracking loops at the receiver are often subjected to dynamic stress and low C/N_0 signals in the weak signal environment. Hence, from the rule-of-thumb tracking threshold criteria as shown in Eq. 2.16, the equivalent noise bandwidth for a loop filter in the PLL/FLL has to be chosen to accommodate the expected signal dynamics for a given C/N_0 level. The optimal tracking loop bandwidth conditioned on the minimization of tracking loop phase and frequency error can be obtained by differentiating $\sigma_{\delta\phi}$ and $\sigma_{\delta f}$ with respect to loop bandwidth and equating it to zero [50], i.e., $\frac{\partial\sigma_{\delta\phi}}{\partial B_{pll}} = 0$ and $\frac{\partial\sigma_{\delta f}}{\partial B_{fll}} = 0$. This yields the following optimal bandwidth expression for second-order PLL and FLL,

$$\begin{aligned}
B_{pll} &= \left(\frac{(2.35\delta\dot{f})^2}{\frac{1}{c/n_0}\left(1+\frac{1}{2Tc/n_0}\right)}\right)^{1/5} \\
B_{fll} &= \left(\frac{(2.35\delta\ddot{f})^2}{\frac{4}{c/n_0}\left(1+\frac{1}{2Tc/n_0}\right)}\right)^{1/5}
\end{aligned} \tag{2.20}$$

Analytical values of an optimal PLL tracking loop bandwidth for low, medium, and high signal dynamics at varying signal power levels and integration time of $T = 20\,\text{ms}$ are shown in Fig. 2.4.

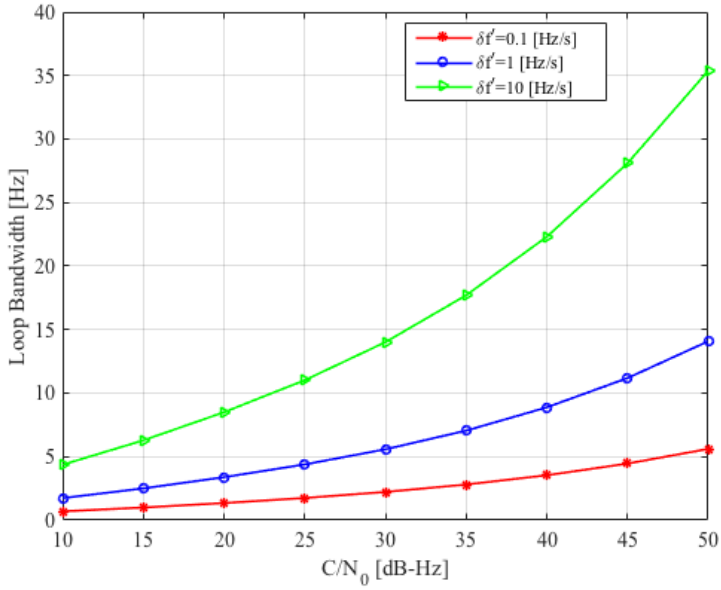

Figure 2.4: Optimal PLL loop bandwidth for varying C/N_0 and signal dynamics.

A narrow loop bandwidth is beneficial at low C/N_0 levels to improve tracking loop noise performance at low signal dynamics, while the wide loop bandwidth is suitable to track high signal dynamics. Finally, the objective of the tracking loop design criteria is to select the lowest bandwidth that is required to accommodate the expected signal dynamics and to meet the tracking loop error criteria. Hence, for an efficient tracking loop operation, the noise bandwidth should be adapted to the received signal C/N_0 value and the changing signal dynamics in real time. For this reason, an adaptive scheme is needed to effectively change the equivalent noise bandwidth with respect to the signal C/N_0 value and signal dynamics estimated using the received signal carrier-phase error measurements.

Now, the discussion is moving on to the next stage of the GNSS receiver, namely the navigation processor. The tracking loop code and carrier-phase output variables are used to generate *pseudorange and range-rate* observations in the navigation processor to compute navigation solution. The mathematical representation of code and carrier-phase pseudorange observations at multiple carrier frequencies is described in the next section.

2.7 Signal observation models

Pseudorange observation can be generated from both code and carrier-phase observations. The code-phase range P_k and carrier-phase range ϕ_k in meters at frequency f_k can be expressed as sum of the true geometric range ρ, error due to satellite clock $c\,(\delta t)$, error due to receiver clock $c\,(\delta T)$, error due to ionosphere I_k, error due to troposphere T_k and range error due to other observation noise ϵ_{P_k} and ε_{ϕ_k},

$$\begin{aligned} P_k &= \rho + c(dt - dT) + I_k + T_k + M_{P_k} + \varepsilon_{P_k} \\ \phi_k &= \rho + c(dt - dT) - I_k + T_k + M_{\Phi_k} + \lambda_k N_k + \varepsilon_{\phi_k} \end{aligned} \tag{2.21}$$

where N_k is the carrier-phase integer ambiguity, λ_k is the wavelength of the frequency f_k; M_{P_k}, M_{Φ_k} are multipath errors in code and carrier-phase range observations respectively.

From Eq. 2.21, it is inferred that code and carrier-phase range observations are corrupted by the same errors. The main difference between the code and carrier-phase range observations is that the code pseudorange observations are coarse and unambiguous, whereas the carrier-phase pseudorange observations are highly precise and ambiguous [12].

Pseudorange rate observation is the change in range between satellite and receiver over an observation interval. The relative motion of satellite and user receiver changes the range and results as Doppler shift in the frequency of the satellite signal. This Doppler shift is observed traditionally by carrier tracking loop. The Doppler frequency is equivalent to the rate of change of the code pseudorange observation or the carrier-phase pseudorange observation over the observation time interval [48],

$$f_{D_k} = \frac{P_k(t_2) - P_k(t_1)}{\lambda_k(t_2 - t_1)} = \frac{\phi_k(t_2) - \phi_k(t_1)}{(t_2 - t_1)} \tag{2.22}$$

The code/carrier-phase pseudorange observation accuracy at each frequency channel is limited by multiple error sources as shown in Eq. 2.21. Some of these errors are correlated across multiple frequency channel observations, while some are not. However, it is necessary to estimate and eliminate pseudorange observation errors to improve the accuracy of position solution. A well-known procedure to estimate correlated errors is by taking observations at two or more frequency channels, then generate a weighted linear combination of observations to eliminate correlated errors as discussed in the following section.

2.7.1 Linear combination of observations

The weighted linear combination of two-frequency signals L_i and L_j code pseudorange observation, P_{ij}, and carrier-phase pseudorange observation, ϕ_{ij}, can be expressed as,

$$\begin{aligned} P_{ij}(t) &= \gamma_{ij} P_i(t) + (1 - \gamma_{ij})\, P_j(t) \\ \phi_{ij}(t) &= \gamma_{ij} \phi_i(t) + (1 - \gamma_{ij})\, \phi_j(t) \end{aligned} \tag{2.23}$$

where $P_i(t)$ is the pseudorange observations of subscripted frequency channel in meters, $\phi_i(t)$ is the carrier-phase range observation of subscripted frequency channel in meters, γ_{ij} is the weight factor to individual signal code and carrier-phase observations. The values for γ_{ij} have to be chosen to preserve the line-of-sight range. The most widely used linear combination of dual frequency observations are ionosphere-free, wide-lane and narrow-lane, which are considered here for the analysis.

From the Eq. 2.23, *ionosphere-free* pseudorange observation can be obtained using linear combination of two-frequency signal observations with corresponding weight factor as

$$\gamma_{IF} = \frac{f_j^2}{\left(f_i^2 - f_j^2\right)} \tag{2.24}$$

The *wide-lane* combination of two-frequency signal code and carrier-phase pseudorange observations can be generated using the weight factor,

$$\gamma_{WL} = \frac{f_i}{(f_i - f_j)} \tag{2.25}$$

Similarly, the *narrow-lane* combination of code and carrier-phase pseudorange observations can be generated using the weight factor,

$$\gamma_{NL} = \frac{f_i}{(f_i + f_j)} \tag{2.26}$$

In standalone multi-frequency receiver, an ionosphere-free linear combination of observations is used to compute the high accuracy position solution. In precise carrier-phase positioning applications, the wide-lane linear combination of observations are used to resolve the integer ambiguity in carrier-phase observations. Finally, the ionosphere-free code/carrier-phase pseudorange observations are used to compute the position solution as discussed in the following section.

2.8 Navigation solution

The most commonly used algorithms for position solution from pseudoranges in GNSS receiver are least-square method [12], [51] and Kalman filter algorithm [52], [53]. In standalone multi-frequency receiver, ionosphere-free code pseudorange observations are used to compute high accuracy position solution. In differential positioning receiver, the ionosphere-free carrier-phase observations are used after resolving the integer ambiguity, for precise and accurate position computation. The ephemerides required to compute the satellite position in multi-frequency receiver can be decoded from any one of multi-frequency channel's navigation data.

The ionosphere-free pseudoranges can be generated by substituting the pseudorange observations at two-frequency channels as given in Eq. 2.21 into Eq. 2.23,

$$\begin{aligned} P_{IF} &= \rho + c(dt - dT) + e_{P_{IF}} \\ e_{P_{IF}} &= \gamma_{IF} e_{P_i} + (1 - \gamma_{IF})\, e_{P_j} \end{aligned} \tag{2.27}$$

where e_{P_i} represents the uncorrelated errors due to troposphere delay, multipath and other observation noise in the subscripted frequency channel, i.e., $e_{P_i} = T_i + M_{P_i} + \varepsilon_{P_i}$

From the ephemerides message, the information about the satellite clock offset, dt and the position of the satellite (X_s, Y_s, Z_s) can be computed. The ionosphere-free pseudorange observations and satellite position information can be used to compute the receiver position using either a least square method or Kalman filter algorithm.

2.9 Summary

In the light of above discussion on multi-frequency GNSS signal characteristics and receiver signal tracking algorithms, some of the factors that determine the receiver tracking loop noise performance are summarized in this section.

- The signal code and carrier-phase tracking loop noise performance is determined by the tracking loop bandwidth, integration time, received signal power levels and dynamics as shown in Eqs. 2.17 and 2.18. The received signal characteristics can not be controlled. Hence, the optimization of the receiver tracking loop bandwidth and integration time may lead to improved tracking loop noise performance.
- A narrow loop bandwidth has benefit in terms of low observation noise in the absence of dynamic stress errors. Hence, the narrow loop bandwidth signal tracking with external signal dynamics information aid lead to improved tracking loop noise performance under dynamic environment.
- The signals designed with higher power have inherent benefit of better tracking loop threshold compared to lower power signals.
- The new GNSS civil signals designed with dual-channels have the benefit of the pilot channel tracking using pure PLL. The pilot channel tracking has an advantage of extra 6-dB tracking threshold compared to data-channel. Furthermore, the pilot channel tracking enables longer coherent integration time to achieve higher sensitivity.
- Regarding the optimum tracking loop design criteria, for an efficient tracking loop operation, it is necessary to adjust the tracking loop bandwidth in response to the received signal power level and dynamics.
- The performance of a linear combination of multi-frequency signals in the observation domain is determined by the individual channel tracking loop noise performance. Hence, it is necessary to analyze the performance of multi-frequency signals in order to find optimum signal combination for an intended application.

3 Performance Analysis of Multi-frequency GNSS Receiver

This chapter presents the performance analysis of multi-frequency GNSS receiver using the different combination of multi-frequency signals in time-varying GNSS signal environment. The criteria to select an optimum combination of two-frequency signals intended for different civilian applications shown in publication [P1] and [P4] are reviewed.

The main contributions of this chapter are as follows:

- Presentation of the key parameters that determine the performance of multi-frequency GNSS receiver.
- Discussion about the factors that influence the performance of GNSS receiver in processing signals received over multiple frequency channels.
- The analysis of the performance of combined multi-frequency signals in the observation domain in terms of observation accuracy, precision, and tracking loop threshold requirement.
- The discussion of the criteria to enable two-frequency signals to complement each other in the observation domain for intended civilian applications.

3.1 Key performance parameters of GNSS receiver

In general, the performance of a GNSS receiver is determined by the signal tracking sensitivity, observation accuracy, and robustness to RF interference. The signal observation accuracy and robustness are closely related to tracking loop noise performance since the receiver tracking loop loses lock if the observation errors exceed a certain threshold [54]. Hence, the GNSS receiver performance is mainly determined by the received signal characteristics and tracking loop performance. The GNSS signals are often subjected to dynamics and low C/N_0 in challenging signal environments such as urban canyon or foliage. Although LOS signal dynamics are common to received multi-frequency signals, the signal C/N_0 varies as each of them are transmitted over different RF channels.

3.1.1 Signal tracking sensitivity

Signal tracking sensitivity is the minimum C/N_0 tracking threshold of the receiver, above which the carrier tracking loop error is maintained below the acceptable error threshold. The signal tracking sensitivity determines the performance of the receiver in a weak signal environment. For a given receiver tracking loop design, the signal tracking loop

threshold is a function of the received signal strength, C/N_0, signal wavelength, and signal dynamics, as shown in Section 2.5. In GNSS receiver, carrier-aided code tracking loop threshold is better than an unaided carrier tracking loop threshold under dynamic environment [54]. Hence, analyzing the carrier tracking loop threshold performance is sufficient to determine the overall receiver signal tracking loop threshold.

The multi-frequency signal carrier tracking loop performance can be evaluated using rule-of-thumb analytical error models as introduced in Eq. 2.10 [13]. For instance, GPS L1, L2C, and L5 signal carrier tracking loop performance is evaluated at low, medium, and higher signal dynamics and varying signal C/N_0, and at a specified tracking loop parameters, i.e. loop BW and PIT.

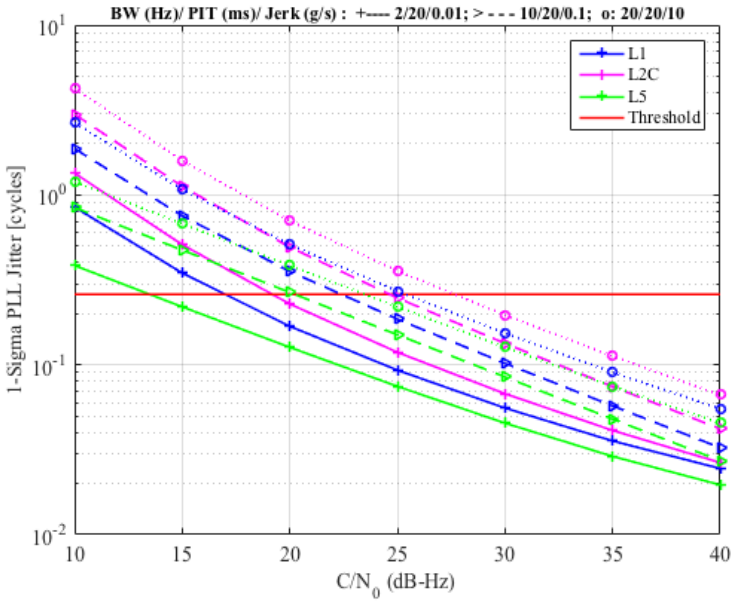

Figure 3.1: 1-sigma carrier-phase error in GPS L1, L2C and L5 signals

Fig. 3.1 illustrates the tracking loop performance of GPS L1, L2C, and L5 signals. The signal tracking loop threshold is the minimum C/N_0 at which the 1-sigma value of PLL error is crossing the tracking error threshold indicated by the red line. The GPS L5 signal with data-less (pilot) channel tracking using pure PLL discriminator has an advantage of additional tracking loop threshold up to 3.5 dB, compared to GPS L1 and L2C data channel tracking using Costas loop discriminator. Furthermore, L1 signal with relatively high received power has better signal tracking sensitivity than L2C data channel. In low signal dynamics tracking using 2 Hz narrow-band PLL, the receiver tracking loop threshold for GPS L1/L2C/L5 signals is about 17/19/14 dB-Hz. For high signal dynamics tracking using 20 Hz wide-band PLL, the receiver tracking loop threshold for GPS L1/L2C/L5 signals is about 25/27/22 dB-Hz.

3.1.2 Observation accuracy

The *accuracy* of signal observation in GNSS receiver is a statistical measure that represents the closeness of the observed range value to the true range between the satellite and

receiver. The pseudorange observation accuracy can be related to the desired position accuracy by the Dilution of Position (DOP), i.e. Position Dilution of Position (PDOP), Horizontal Dilution of Precision (HDOP) [55]. If it is assumed that PDOP=2, then the position accuracy requirement of 5 m translates to a pseudorange accuracy requirement of $\leq$2.5 m. The position accuracy is a primary performance parameter specified in most of the LBS services such as emergency call location, surveying, autonomous car and so on. The pseudorange observation accuracy is determined by the accuracy of code and carrier-phase observations. The received GNSS signal code and carrier-phase observations are corrupted by multiple error sources such as satellite and receiver clock offsets, atmospheric errors, multipath, and RF interference. Some of these observation errors are correlated across multiple frequency channels, while some are uncorrelated. In single-frequency receiver, these errors are partially eliminated either by using error information decoded from satellite navigation message or external aiding from augmented services such as SBAS and Differential GPS (DGPS) etc. In multi-frequency receiver, the spatial and temporal correlation of observation errors at multiple frequency channels can be utilized to estimate and eliminate common-mode observation errors. The uncorrelated observation errors still remain and influence the observation accuracy and precision.

3.1.3 Observation precision

Observation precision represents the deviation of observations from the mean value of the observations. In GNSS receiver, the pseudorange observation precision is determined by the random noise and multipath. The received signals from multiple radio frequency bands typically encounter different multipath channels and RF interference. The size of the multipath errors in multiple frequency tracking channels may also be different since higher frequency signals tend to experience less multipath. Multipath is the major source of error in code-phase observations. Furthermore, because of the relative movement between the satellite and user receiver, the multipath will, in general, be time-varying.

The Multipath Error Envelope (MEE) is used in general to evaluate the multipath performance of various signals and receiver tracking algorithms, [56], [57], [58].

From Fig. 3.2, it is inferred that the GNSS receiver can effectively mitigate the multipath signal if the multipath delay is greater than 1.5 times chip duration [57]. The influence of multipath in code-phase observation is mainly dependent on the code rate of signals and code correlator spacing in tracking loops. Hence, the signals with higher chip rates and receiver tracking loops with narrow correlators have less influence of multipath, see [59]. For instance, multipath error in L5 code-phase observations is 10 times smaller than that of L1 and L2C signal code-phase observations. The receiver tracking loop with 0.1 chip correlator spacing has a lower multipath error compared to the one with 0.5 chip spacing.

3.1.4 Robustness to interference

The *robustness* of GNSS receiver is the ability to withstand both intentional and unintentional RF interference. Robustness is the most critical parameter in safety-of-life applications, which means that protection against interference is desirable. In GNSS receiver, robustness to RF interference is determined by the received signal C/N_0 and signal tracking loop threshold. As discussed earlier, the receiver code and carrier tracking loop threshold is in turn determined by the pre-detection integration time, phase discriminator performance and loop filter BW. The narrow loop BW signal tracking with external Doppler aiding, has better tracking loop threshold compared to an unaided signal tracking

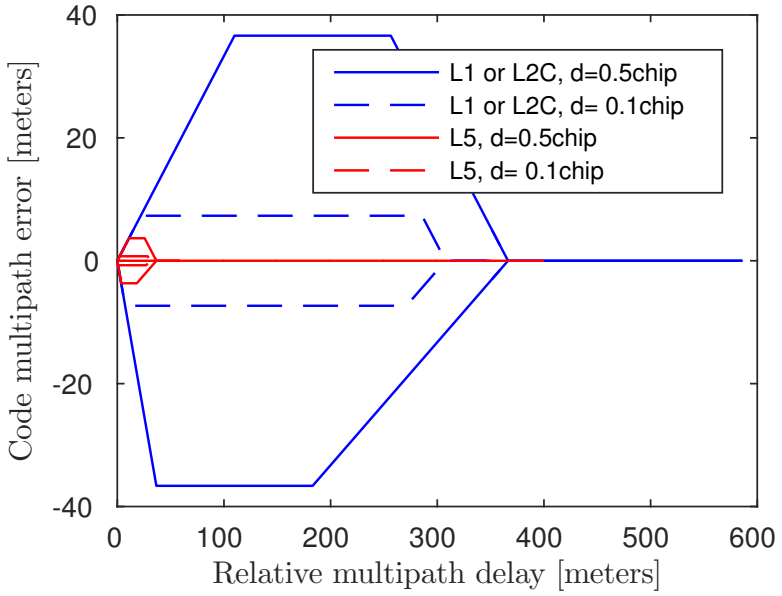

Figure 3.2: GPS L1, L2C, and L5 signal code multipath error versus relative multipath delay at fixed relative multipath amplitude of 0.5 and correlator spacing of 0.5 and 0.1 chip

loop [13]. The improved tracking loop threshold enhances the robustness performance of the receiver.

Robustness to RF interference:

The GNSS receiver robustness to RF interference is evaluated by the tolerable Jammer-to-Signal carrier power ratio (J/S) performance. An in-band RF interference in GNSS receiver channel causes the received signal unjammed C/N_0 to reduce to an effective carrier-to-noise ratio, $(C/N_0)_{eff}$. A characterization of GPS receiver performance during interference is studied in [60]. When the RF interference causes the effective C/N_0 to reduce to the tracking loop threshold, then the difference between the unjammed C/N_0 and effective C/N_0 is the J/S threshold of the receiver channel, [60]

$$\frac{J}{S} = Q_J R_c \left(\frac{1}{(C/N_0)_{eff}} - \frac{1}{C/N_0} \right) \tag{3.1}$$

where C/N_0 is the unjammed carrier-to-noise ratio; J/S is the jammer-to-signal carrier power ratio; R_c code rate of the PRN code. Q_J is a jamming-resistance quality factor, Q_J=1 for Continuous Wave (CW), 1.5 for matched spectrum and 2 for Band Limited White Noise (BLWN);

For instance, the J/S performance of GPS L1, L2C, and L5 signals subjected to three types of RF interference wave-forms is shown in Fig 3.3.

For the same receiver tracking loop design, the GPS L5 signal with 10 times higher chip rate and more received power than GPS L1 signal has the benefit of a higher value of $Q_J R_C$ factor. Hence, the GPS L5 signal is more immune to RF interference than other

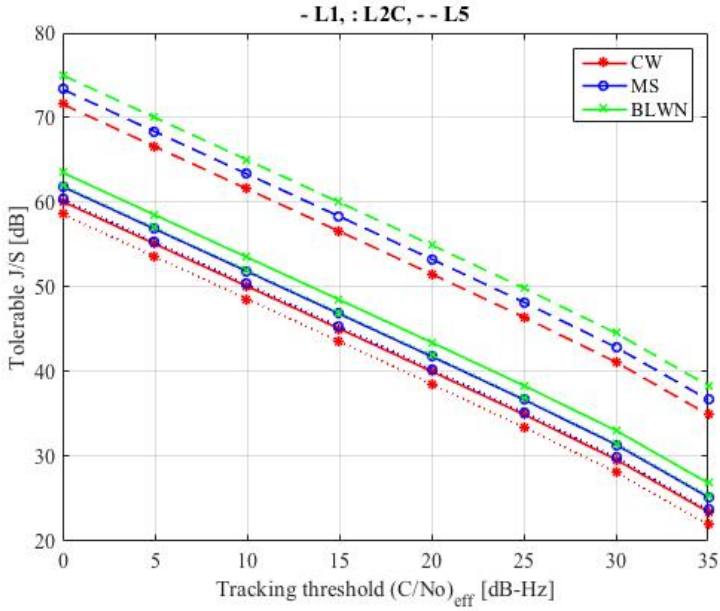

Figure 3.3: Tolerable J/S as a function of receiver tracking threshold in GPS L1, L2C and L5 signals at C/N_0=45 dB-Hz

frequency signals in the GPS system. From the analytical results shown in Fig. 3.3, GPS L5 signal has an extra jamming margin compared to L1 and L2C signals under the influence of same interference conditions.

Robustness to ionosphere scintillation:

Ionospheric scintillation is an unintentional RF interference to the GNSS receiver. Ionospheric scintillations are rapid temporal fluctuations in both amplitude and phase of trans-ionospheric GNSS signals caused by the scattering of irregularities in the distribution of electrons encountered along the radio propagation path. The most severe scintillations are observed near the poles and near the equator [61]. Equatorial amplitude scintillation affects both code and carrier tracking and degrades code and carrier-phase range measurements. Equatorial phase scintillation adversely affects the operation of a receiver's PLL and leads to carrier cycle slips, navigation data bit errors, and complete loss of carrier lock.

A characterization of GPS L1 C/A receiver performance during ionosphere scintillation is studied in [62], [63]. After GNSS modernization, the influence of ionosphere scintillation at L1, L2, and L5 frequency bands is characterized by [64]. The GPS L1, L2, and L5 signal tracking performance during scintillation is assessed by analyzing the experimental data collected during the solar maximum period in [19]. These studies have concluded that the low carrier frequency signals, L2C and L5 tracking is less robust to scintillation than GPS L1 signal, despite the advanced signal characteristics such as high code rate and power.

By considering the diversity in the performance of multi-frequency GNSS signals as discussed above, it is necessary to select a combination of signals in GNSS receiver leading to an optimum performance of each signal for an intended application. Hence,

the performance of combination of multiple frequency signals in the observation domain is analyzed in the following section.

3.2 Performance of linear-combination of multi-frequency signals

In conventional multi-frequency GNSS receiver, multiple frequency channels are tracked independently and then the code/carrier-phase pseudorange observations are linearly combined to eliminate correlated errors as discussed in Section 2.7.1. A weighted linear combination of two-frequency channel code/carrier-phase observations are often used for different purpose in GNSS receivers. Out of three to four civil signal frequencies available from each GNSS system, a number of signal combinations can be generated. However, it is necessary to find an optimal multi-frequency signal combination for an intended application. In standalone kinematic positioning, code-phase observations are preferred to carrier-phase observations, due to lack of integer ambiguity and cycle slip issues. In precise positioning applications, carrier-phase observations are preferred after resolving the integer ambiguity using differential positioning techniques or Precise Point Positioning (PPP) techniques. Now, in order to select the optimal signal combination, it is necessary to assess the noise variance of a dual-frequency signal combination as discussed in the following section

3.2.1 Noise variance in linear combination of observations

By applying the law of noise variance propagation, 1-sigma error in a combined two-frequency signal code and carrier-phase pseudorange observations as shown in Eq. 2.23 can be expressed as [12],

$$\begin{aligned} \sigma_{P_{ij}} &= \sqrt{\gamma_{ij}^2 \sigma_{P_i}^2 + \left(1-\gamma_{ij}\right)^2 \sigma_{P_j}^2} \\ \sigma_{\phi_{ij}} &= \sqrt{\gamma_{ij}^2 \sigma_{\phi_i}^2 + \left(1-\gamma_{ij}\right)^2 \sigma_{\phi_j}^2} \end{aligned} \tag{3.2}$$

Where $\sigma_{P_{ij}}$ is the 1-sigma error in a linear combination of code-phase observation, $\sigma_{\phi_{ij}}$ is the 1-sigma error in a linear combination of carrier-phase observation. As shown in Eq. 3.2, the combined signal observation noise is the sum of the amplified observation noise in each frequency channel. The linear combination of signal observations remove the common-mode errors in order to improve the observation accuracy, but at the expense of increased uncorrelated errors.

3.2.2 Precision of the combined signal observation

As discussed earlier, the precision of the signal observation is determined by the random noise and multipath in the received signal. Hence, the precision performance of a linear combination of observations is analyzed using MEE. For instance, multipath error in ionosphere-free pseudorange observations shown in Fig. 3.4 is significantly higher than the multipath in single-frequency channel observations, shown in Fig. 3.2. The multipath in L1/L2C and L2C/L5 ionospheric-free observations is more dominant than L1/L5 signal combination, due to the relatively slower chip rate of L1 and L2C signals and also the high value of amplification factor, γ_{ij}. The combined signal observation precision is

mainly influenced by the less precise signal observations. For example, the L1/L5 signal code pseudorange observation precision is determined by the less precise L1 pseudorange observations.

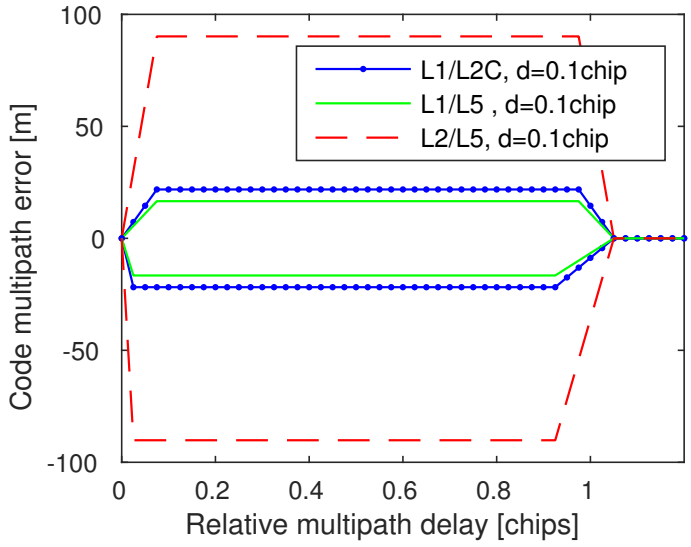

Figure 3.4: Comparison of iono-free code range multipath error variation with relative multipath delay

3.2.3 Tracking loop threshold of the combined signal

According to Eq. 3.2, at lower C/N_0, the observation error of the combined signal increases due to the observation errors from the channel of lower tracking loop threshold. In order to maintain the combined signal observation error within the operational limits, it is necessary to set the tracking threshold in each frequency channel with respect to the combined signal observation error limit. By considering this criterion, the effective signal tracking threshold requirement for two-frequency channels reduces to that of lower performance channel. For instance, in the case of GPS L1/L5 signals, combined solution tracking threshold is determined by the L1 signal. As a result, the process of combining multiple signals in the observation domain improves the observation accuracy at the expense of degradation in the signal tracking threshold performance. This limits the signal tracking sensitivity and robustness to interference.

The linear combination of multi-frequency signal code pseudorange observations is dominated by the amplification of multipath and observation noise in each frequency channel. To reduce the multipath error in code pseudorange observations, carrier smoothing algorithm is a well known signal processing technique [65] employed in GNSS receivers, which is reviewed in the following section.

3.3 Carrier smoothing algorithm

The code-phase observation noise and multipath can be reduced using precise delta carrier-phase observations and carrier smoothing algorithm, also known as Hatch filter

introduced by Ronald Hatch in [65]. The advantage of this procedure is that the carrier-phase observations are more precise and have low multipath than code-phase observations. From the Eq. 2.22, the code pseudorange and delta carrier-phase observations can be combined to obtain precise and unambiguous pseudorange observations as,

$$\begin{aligned} P_{SM}(t+1) &= W_t P(t+1) + (1 - W_t)(P_{SM}(t) + \lambda \Delta\phi(t+1)) \\ \Delta\phi(t+1) &= \phi(t+1) - \phi(t) \end{aligned} \tag{3.3}$$

where $P_{SM}(t)$ smoothed pseudorange in meters, $P(t)$ code pseudorange in meters, $\phi(t)$ is carrier-phase in cycles and λ is its wavelength; W_t represents the smoothing weight factor, commonly taken as the reciprocal of the current epoch and t is the epoch index. For the first epoch, weight factor set to 1 gives the full weight to code pseudorange. For the subsequent epochs, the weight of the code range is continuously reduced by a value and the relative weight of carrier-phase observations is increased. The amount of reduction of the weight factor from epoch to epoch controls the behavior of the algorithm. The carrier smoothing procedure in Eq. 3.3 is limited to short time intervals due to ionosphere delay divergence in single-frequency code and carrier-phase observations, which gives rise to an error proportional to the smoothing filter time constant.

3.3.1 Divergence-free carrier smoothing algorithm

The limitation of ionosphere divergence effect in carrier smoothing process can be overcome by making use of either ionosphere-free or ionosphere-delay matched code-carrier-phase observations of two-frequency signals. The Divergence-free (DF) smoothing and ionosphere-free smoothing processes for dual-frequency signals were introduced in [66]. In ionosphere-free smoothing, ionosphere error is removed from the smoothed pseudoranges. In DF smoothing process, the effects of the ionospheric divergence are removed, but the instantaneous ionospheric delay remains in the smoothed pseudorange observations [67]. The dual-frequency signal code and delta carrier-phase observations can be linearly combined to generate smoothed pseudorange observations, P_{SM} as,

$$\begin{aligned} P_{SM}(t+1) &= W_t P_{ij}(t+1) + (1 - W_t)(P_{SM}(t) + \lambda \Delta\phi_{ij}(t+1)) \\ P_{ij}(t) &= \gamma_{ij} P_i(t) + (1 - \gamma_{ij})\, P_j(t) \\ \Delta\phi_{ij}(t) &= \gamma_{ij} \Delta\phi_i(t) + (1 - \gamma_{ij})\, \Delta\phi_j(t) \end{aligned} \tag{3.4}$$

Where $P_i(t)$, is the pseudorange observation of subscripted signal, $\Delta\phi_i(t)$, is the carrier Doppler observation of subscripted signal. The values for γ_{ij} to be chosen to preserve the line-of-sight range and to eliminate the ionospheric-divergence effect in smoothing process as discussed in [67].

Ionosphere-free smoothing

In ionosphere-free smoothing, ionosphere-free combination of code-phase observations are smoothed using ionosphere-free delta carrier-phase observations by appropriate weight coefficients given in Eq. 2.24,

$$P_{IFS}(t+1) = W_t P_{IF}(t+1) + (1 - W_t)(P_{IFS}(t) + \lambda \Delta\phi_{IF}(t+1)) \tag{3.5}$$

where P_{IFS} is the Ionosphere-free smoothed pseudorange (IFS) observations; P_{IF} is the ionosphere-free combination of code-phase observations; $\Delta\phi_{IF}$ is the ionosphere-free combination of delta carrier-phase observations.

Divergence-free smoothing

In DF smoothing, the weight coefficients have to be chosen to generate ionosphere delay matched code and carrier-phase observations. For instance, ionosphere delay in wide-lane carrier-phase observations is matched to that of narrow-lane code-phase observations. Hence, the narrow-lane code-phase observations can be smoothed using ionosphere delay matched wide-lane carrier-phase observations to generate ionosphere divergence-free smoothed pseudorange observations. Similarly, the wide-lane code pseudoranges can be smoothed using ionosphere delay matched narrow-lane carrier-phase observations.

$$P_{WLS}(t+1) = W_t P_{NL}(t+1) + (1 - W_t)(P_{WLS}(t) + \lambda\Delta\phi_{WL}(t+1)) \tag{3.6}$$

$$P_{NLS}(t+1) = W_t P_{WL}(t+1) + (1 - W_t)(P_{NLS}(t) + \lambda\Delta\phi_{NL}(t+1)) \tag{3.7}$$

where P_{WLS} is the wide-lane carrier phase smoothed narrow-lane pseudorange (WLS) observations; P_{NLS} is the Narrow-lane carrier phase smoothed wide-lane pseudorange (NLS) observations; P_{NL}, P_{WL} are narrow-lane and wide-lane combination of code-phase observations respectively; $\Delta\phi_{NL}$, $\Delta\phi_{WL}$ are narrow-lane and wide-lane combination of delta carrier-phase observations respectively.

The ionosphere-free and divergence-free carrier smoothing process improves the precision of absolute code-phase range observations. This procedure, in turn, generates some extra errors in smoothed pseudorange observations. The propagation of errors in smoothed pseudorange observations due to the combined code and delta carrier-phase observations is assessed in the following section.

3.3.2 Error assessment in smoothed pseudorange observations:

As it is discussed in [67], IFS observations are free of ionosphere delay bias, but has the code and carrier-phase observation noise. The Divergence-free smoothed pseudorange (DFS) observations have errors from the code and carrier-phase observation noise and also ionosphere bias error in the code-phase observations.

In the steady state, $(1 - W_t) \approx 1$, then, from Eq. 3.4, 1-sigma error in smoothed pseudorange observation, $\sigma_{P_{SM}}$, can be written as,

$$\sigma_{P_{SM}} = \sqrt{\sigma^2_{P_{ij}} + \sigma^2_{\Delta\phi_{ij}}} \tag{3.8}$$

where $\sigma_{P_{ij}}$, $\sigma_{\Delta\phi_{ij}}$ are the 1-sigma error in linear combination of code and delta carrier-phase observations respectively.

Ionosphere delay bias, δI, in smoothed pseudorange observations,

$$\delta I = [\gamma_{ij} I_i + (1 - \gamma_{ij}) I_j] \tag{3.9}$$

where I_i is the ionosphere delay in code-phase observation of the subscripted frequency channel.

The errors in the linear combination of code/carrier-phase observations are sum of the amplification of errors in the code/carrier-phase observations of two-frequency signals as shown in Eq. 3.2.

From the above error assessment, the total errors in IFS observations are illustrated in Fig. 3.5. In the first few epochs, the IFS observation error is due to ionosphere-free code-phase observation noise. After the convergence of smoothing filter, the IFS observation error is reduced to the ionosphere-free carrier-phase observation noise. The IFS observations are offset from the true range by the initial ionosphere-free code-phase observation noise.

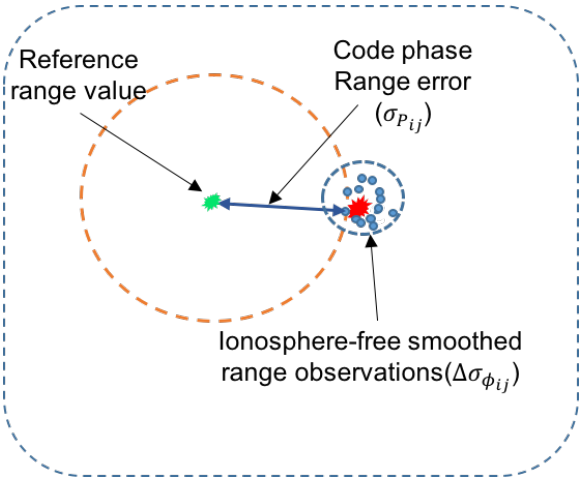

Figure 3.5: Errors in IFS observations

The total errors in DFS observations are illustrated in Fig. 3.6. In DFS observations, initial range error is due to the code-phase observation noise and its ionosphere bias. The carrier smoothing process will improve the precision of range observations in the subsequent epochs. The DFS observations are offset from the true range by the code-phase observation noise and ionosphere-bias error.

For experimental verification, the GPS L1/L5 signal code and carrier-phase observations are recorded using Javad DELTA receiver from block-IIF satellites. These observations are processed using multi-frequency GNSS receiver post-processing software developed in this project. The errors in smoothed pseudorange observations generated using combination of L1/L5 signal code and carrier-phase observations are shown in Fig. 3.7. In the first few epochs, smoothed pseudorange observation error being high due to the code-phase observation noise. Subsequently, after few epochs, pseudorange error is reduced to the carrier-phase observation noise.

From Fig. 3.7, it is inferred that the WLS observations have a minimum code-phase noise and the highest ionosphere delay bias as per the Eq. 3.9, which is shown in [P4]. The IFS is free of ionosphere error and has high code-phase noise. The ionosphere delay bias error leads to less accurate pseudorange observations, while high code-phase noise results in less precise pseudorange observations. Hence, one has to choose between ionosphere-bias error and observation noise to make use of smoothed pseudorange observations for the intended

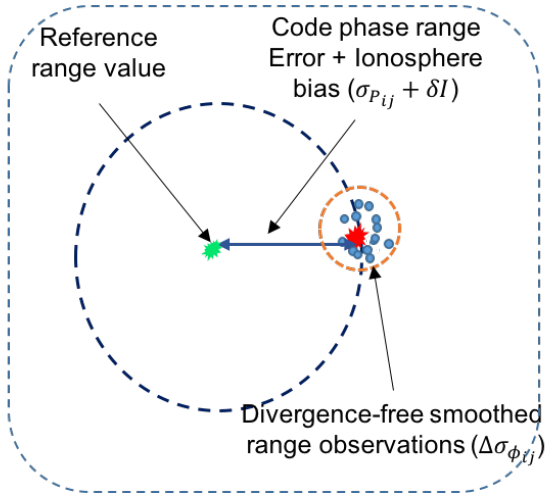

Figure 3.6: Errors in DFS observations

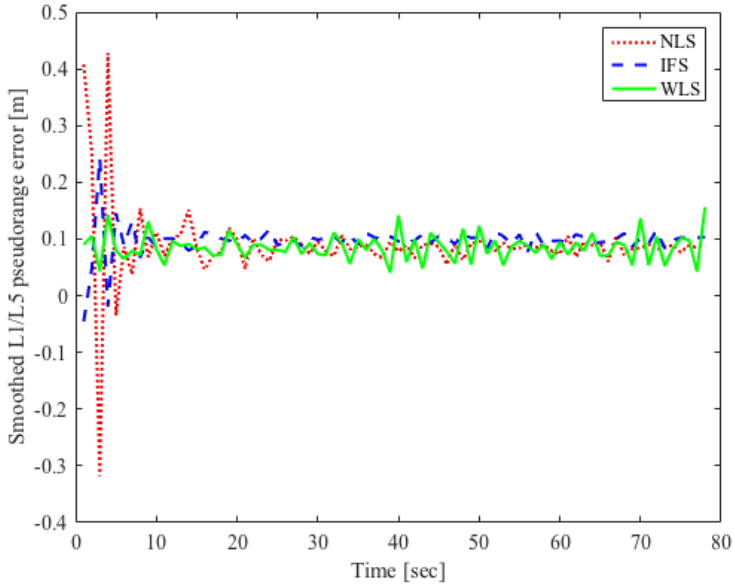

Figure 3.7: Errors in smoothed pseudorange observations of L1/L5 signals

application. The quantitative values of ionosphere-bias error and observation noise in smoothed pseudorange observations is again determined by the choice of two-frequency signals. Hence, it is necessary to select a combination of two-frequency signals to minimise the ionosphere-bias error and observation noise in smoothed pseudorange observations.

3.4 Criteria to select two-frequency signals

Out of three civil signals in GPS L1/L2C/L5 and GALILEO E1/E5/E6, a user has a number of potential ways to form a linear combination of observations to serve the different purpose in civilian applications. The criteria to select an optimum combination of two-frequency signals are specific to the intended application. For instance, the ionosphere-free signal combination requires two-frequency signals that are widely spaced in RF spectrum to have low noise amplification factor. The wide-lane combination require two-frequency signals closely spaced in RF spectrum, to form large wavelength lanes for the fast convergence of integer ambiguity resolution in carrier-phase observations.

Ionosphere-free signal combination

Although three or four carrier signals are available, in general, most of the standalone kinematic applications get benefit from two-frequency signals to estimate and eliminate ionosphere delay error in the signal observations. In view of this requirement, the analytical and experimental analysis is carried out to find an optimum ionosphere-free signal combination for standalone dual-frequency receiver in [P3]. For instance, out of three signal combinations in GPS and GALILEO system, the GPS L1/L5 and GALILEO E1/E5 signal combination have the benefit of advanced L5/E5 signal characteristics and low noise amplification factor. Hence, the GPS L1/L5 and GALILEO E1/E5 is an optimal signal combination for ionosphere-free position solution in standalone dual-frequency receiver.

Integer Ambiguity Resolution (IAR)

In general, the carrier-phase integer ambiguity is resolved by the geometry-free technique using a linear combination of absolute code-phase and ambiguous precise carrier-phase observations. The ionosphere bias in narrow-lane code-phase observations is matched to the ionosphere bias in wide-lane carrier-phase observations. Hence, the narrow-lane code-phase and wide-lane carrier-phase observations are generally called ionosphere delay matched code-carrier-phase observation models. The use of ionosphere bias matched linear combination of code-carrier-phase difference observations in ambiguity solution eliminates the ionosphere bias error. However, this approach is limited by the high code-phase observation noise and multipath. The code-phase observation noise and multipath can be reduced through carrier smoothing process as discussed in the previous section. The DF smoothed pseudoranges are more precise to set the ambiguities in carrier-phase observations [67]. The feasibility and success rate of using smoothed code-phase observations in wide-lane integer ambiguity solution is analyzed in [P4].

As shown in [P4], the low noise WLS observations are suitable to fix wide-lane carrier-phase integer ambiguity. The ionosphere-free wide-lane integer ambiguity estimation using WLS pseudorange observations can be given by,

$$\hat{N}_{WL} = \phi_{WL} - \frac{P_{WLS}}{\lambda_{WL}} \tag{3.10}$$

From the law of noise variance propagation, 1-sigma error in integer ambiguity estimation can be expressed as,

$$\sigma(\hat{N}_{WL}) = \sqrt{\sigma^2(\phi_{WL}) + \frac{\sigma^2(P_{WLS})}{\lambda_{WL}^2}} \tag{3.11}$$
$$\sigma(\hat{N}_{WL}) \approx \frac{\sigma(P_{WLS})}{\lambda_{WL}}$$

As shown in Eq. 3.11, the wide-lane integer ambiguity error variance is determined by the WLS observation noise variance to wide-lane wavelength ratio. The WLS observation variance is in turn determined by the narrow-lane code-phase observation noise before the convergence of the smoothing filter. The integer ambiguity success rate in the first few epochs is dependent on the narrow-lane code-phase observation noise to wide-lane wavelength ratio. Hence, the combination of two-frequency signals, which have a low value of narrow-lane code-phase noise to wide-lane wavelength ratio tends to have high success rate in the ambiguity solution.

For instance, in the GPS system, using three signal frequencies, three wide-lane combinations are optimal for ambiguity resolution in terms of minimum observation noise, as concluded in [46]. The noise variance and success rate in geometry-free and ionosphere-free integer ambiguity solution in three wide-lane carrier-phase observations are analyzed in [P4]. Out of three wide-lanes, the L2/L5 signal combination has the advantage of the low value of narrow-lane code-phase observation noise to extra wide-lane wavelength ratio. As a result, the extra wide-lane formed using L2C/L5 signals has low value of integer ambiguity error variance, which is suitable to attain high success rate in fixing integer ambiguity instantaneously. The other two wide lanes L1/L2C and L1/L5 are limited by the high value of code-phase observation noise to wavelength ratio in the first few epochs. After the convergence of smoothing filter, three wide lanes tend to have a similar success rate in integer ambiguity resolution. In standalone precise point positioning, the GPS L2/L5 signal combination is more suitable for geometry-free and ionosphere-free wide-lane fixing followed by the narrow-lane carrier-phase ambiguity solution.

3.5 Summary

This chapter has presented the performance analysis of multi-frequency GNSS signals and performance benefits and limitations of combined multi-frequency signals in the observation domain. The summary of this chapter is presented in this section.

- The multiple frequency GNSS signals designed with unique signal characteristics and transmitted at different RF spectrum have significant performance differences at the receiver [P1]. For example, the signals with higher power and higher chip rate have better multipath mitigation and precise range measurements. The signals defined with dual-channels (data+pilot) have the benefit of pilot channel tracking to achieve extra tracking threshold of 6-dB. This, in turn, enhances the signal tracking sensitivity. The signals transmitted at higher RF frequencies are robust to ionosphere scintillation compared to signals at low RF carrier frequency. Finally, the diversity in the performance of multi-frequency GNSS signals can be utilized in receiver to complement each other in challenging signal conditions.
- Out of three or four signal frequencies available from each GNSS system, not all signals or combination of signals are suitable for every application. The performance of multi-frequency signals in the observation domain is analyzed to find

optimum two-frequency signals for ionosphere-free position solution in [P1] and for integer ambiguity resolution in carrier-phase observations in [P4]. For instance, the GPS L1/L5 and GALILEO E1/E5 signal combination are found as optimum for ionosphere-free positioning in-terms of observation noise, which is also verified through experiments in [P1]. The GPS L2/L5 signal combination is optimal for wide-lane integer ambiguity resolution instantaneously with high success-rate as shown in [P4].

- The classical multi-frequency signal processing algorithms discussed earlier are designed to enable the multiple frequency signals to complement each other in the observation domain. These approaches are defined to combine the multi-frequency channel code and carrier-phase observations to remove common-mode errors in order to improve the observation accuracy and precision. The performance of these approaches is severely limited in the weak signal conditions. This happens because of combining the signals of different tracking loop noise performance. As a result, uncorrelated errors in the combined signal observation increases. The traditional multi-frequency signal processing methods have improved the observation accuracy at the expense of degradation in the combined signal tracking threshold and observation precision.

- In GNSS receiver, the code and carrier tracking loop output variables are used to generate range and range rate observations. Therefore, the signal observation noise performance is determined by the signal tracking loop noise performance. It is necessary to devise signal processing techniques to enable the multiple frequency channels to complement each other to enhance signal tracking performance in challenging signal conditions. This will improve the overall multi-frequency receiver sensitivity and position accuracy.

4 Dual-frequency Signal Processing Architecture

The GNSS receiver performance is majorly determined by the signal tracking loop performance. Therefore, it is necessary to put an effort to improve the individual frequency channel tracking loop performance before combining signals in the observation domain. This chapter presents the contribution of [P2], which was aimed to enhance the dual-frequency signal tracking sensitivity and observation noise performance by common Doppler estimate based dual-frequency signal tracking loop. The outline of this chapter is as follows,

- Presentation of the details about the proposed dual-frequency signal processing architecture for standalone dual-frequency receiver published in [P2].
- Discussion of the common Doppler-aided dual-frequency signal tracking loop architecture.
- The performance of the proposed signal processing architecture is validated using experimental results by collecting live satellite signal over GPS L1 and L5 signal frequencies.

4.1 Introduction

By making use of coherency in multiple frequency signal generation in the satellite as shown in Section 1.3.4, a dual-frequency signal processing architecture is proposed to enhance the individual channel tracking performance and to reduce the noise in the linear combination of observations. In order to evaluate the proposed dual-frequency signal processing architecture, GPS L1/L5 and GALILEO E1/E5 signals are considered as specific examples. Because these two signal combinations were found to be the optimum for ionosphere-free position solution as shown in [P1] and also according to the optimal criteria to select two-frequency signals discussed in Section 3.4. The proposed approach is suitable to process any combination of two-frequency signals in multi-frequency GNSS system, in normal ionosphere conditions, i.e., in the absence of ionosphere scintillation.

In a conventional dual-frequency receiver, the performance of L1/L5 and E1/E5 combined signal position solution is limited by the low-performance L1/E1 signal as shown in Section 3.2. In order to improve the performance of the dual-frequency signal solution, it is necessary to improve the L1/E1 signal tracking loop performance to be on par with the L5/E5 signal. By taking advantage of GPS L5/GALILEO E5 signal tracking loop performance as it was shown in Figs. 3.1, 3.2 and 3.3, a dual-frequency signal

processing architecture is proposed with an aim to enhance the L1/E1 signal tracking loop performance and subsequently to reduce the noise in ionosphere-free pseudorange observations. The functional block diagram of the proposed dual-frequency signal processing architecture is shown in Fig. 4.1.

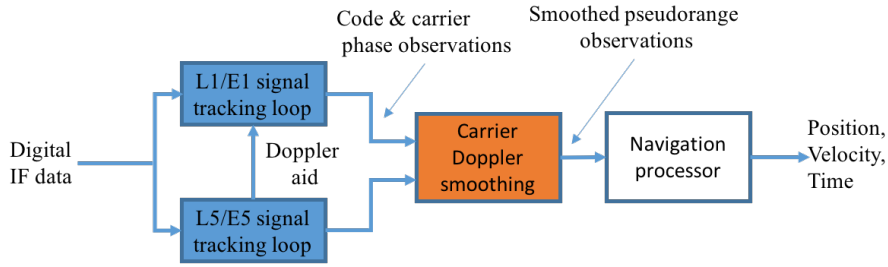

Figure 4.1: Dual-frequency signal processing architecture

By making use of the linear relation in LOS geometric Doppler shift across multi-frequency signals shown in Section 1.3.4, two-frequency signals can be tracked using common Doppler shift estimate. There are many approaches to estimate LOS Doppler shift common to two-frequency signals, either by using single-frequency channel discriminator output [17] or by weighted linear combination of two-frequency channel discriminator outputs as discussed in [68], [27]. In normal ionosphere conditions, L5/E5 signal tracking loop noise performance is always better than for L1/E1 signal, hence, it is beneficial for a dual-frequency receiver to use L5/E5 channel discriminator output to estimate the Doppler shift. Hence, the L5/E5 channel is chosen to provide Doppler aid to the L1/E1 channel tracking loop. As a result, the two-frequency signal tracking using the low-noise L5/E5 signal Doppler observation enhances the L1/E1 signal tracking loop noise performance. Furthermore, two-frequency signals tracked using common Doppler estimate tend to have correlated observation errors, which will indeed cancel out when linearly combined in the observation domain, i.e., ionosphere-free, wide-lane etc. This inturn will reduce the noise in linear combination of ionosphere-free code pseudorange observations. Additionally, code pseudorange smoothing using carrier Doppler observations improves the precision of the final position solution. The cycle slips encountered in carrier-phase observations can be neglected by making use of the carrier Doppler observations in the smoothing process [69], [70].

The Doppler-aided two-frequency signal tracking loop architecture is discussed in the following section.

4.2 Doppler-aided two-frequency signal tracking

The GNSS receiver tracking loop performance can be improved under dynamic environment through external aiding of signal dynamics information from inertial sensors [54], [15]. Similarly, the signal tracking loop performance in the dual-frequency receiver can be improved under dynamic environment through an inter-band Doppler aiding process [17]. In inter-band Doppler aiding, a signal channel of relatively higher C/N_0 tracking threshold provides Doppler aid to the lower performance channel tracking loop. As a result, the aided signal tracking loop filter bandwidth is narrowed to track residual phase variations. The narrow bandwidth signal tracking improves the C/N_0 tracking loop threshold of

the aided signal. This, in turn, enhances the aided signal tracking loop sensitivity and robustness to interference.

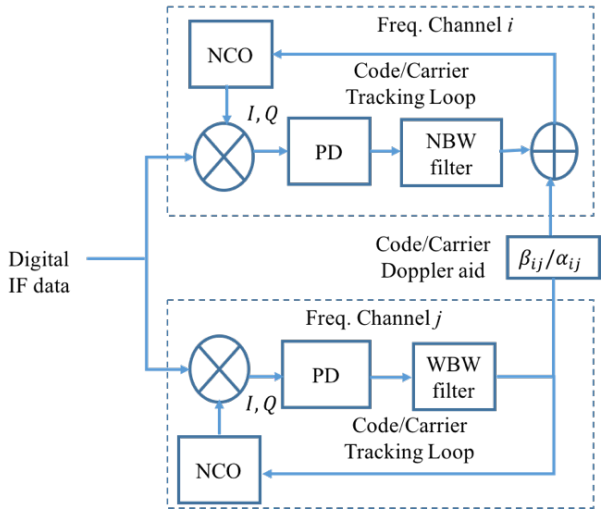

Figure 4.2: Doppler aided tracking loop architecture

The linear relation in multiple frequency channel code and carrier frequencies is utilized to provide inter-band Doppler estimate aid between the tracking loops within a dual-frequency receiver channels. For example, if two-frequency signals are assumed as L_i and L_j, out of which a low-noise signal L_j provides a Doppler aid to L_i signal tracking loops. A scaled Doppler value of L_j signal code and carrier-phase tracking loop filter output is passed on to the L_i signal code and carrier loop update function as an external aiding as shown in Fig. 4.2. Hence, the code and carrier Doppler value in the aided signal L_i can be expressed compactly in matrix form as

$$\begin{bmatrix} f_{cdL_i} \\ f_{DL_i} \end{bmatrix} = \begin{bmatrix} \beta_{ij} & 0 \\ 0 & \alpha_{ij} \end{bmatrix} \begin{bmatrix} f_{cdL_j} \\ f_{DL_j} \end{bmatrix} + \begin{bmatrix} \Delta f_{cdL_i} \\ \Delta f_{DL_i} \end{bmatrix} \tag{4.1}$$

$$\beta_{ij} = \frac{f_{cL_i}}{f_{cL_j}}; \alpha_{ij} = \frac{f_{L_i}}{f_{L_j}}$$

Where f_{cL_i}, f_{L_i} are the code and carrier frequency of the subscripted channel;
f_{cdL_i}, f_{DL_i} are the Doppler shift in the code and carrier frequency of the subscripted channel;
Δf_{cdL_i}, Δf_{DL_i} are the residual Doppler shift in the code and carrier frequency of the subscripted channel;

From Eq. 4.1, 1-sigma observation noise in the aided signal code and carrier tracking loop can be expressed as

$$\begin{aligned} \sigma_{P_{i-A}} &= \sqrt{\beta_{ij}^2 \sigma_{P_j}^2 + \sigma_{P_{i-NL}}^2} \\ \sigma_{\phi_{i-A}} &= \sqrt{\alpha_{ij}^2 \sigma_{\phi_j}^2 + \sigma_{\phi_{i-NL}}^2} \end{aligned} \tag{4.2}$$

The total noise in the aided signal tracking loop, $\sigma_{P_{i-A}}$, is proportional to the noise in the narrow tracking loop, $\sigma^2_{P_{i-NL}}$, and the noise induced from the inter-band Doppler aid, $\beta^2_{ij}\sigma^2_{P_j}$. The extra noise induced from Doppler aid [17] has both systematic and random noise components, i.e., $\sigma^2_{P_j} = \sigma^2_{P_{j-r}} + \sigma^2_{P_{j-s}}$. The systematic error component, $\sigma^2_{P_{j-s}}$, which is correlated across the two-frequency signal observations will tend to reduce in the linear combination of observations due to cancellation. However, the random noise component, $\sigma^2_{P_{j-r}}$, still remains and gets amplified in combined signal observations. Hence, to benefit from this architecture, it is necessary to choose relatively low observation noise frequency channel to estimate the common Doppler shift.

The improvement in aided signal C/N_0 tracking loop threshold can be expressed as the ratio of the wider-loop bandwidth (WBW) employed in scalar tracking loop architecture to the narrow-loop bandwidth (NBW) in Doppler-aided tracking loop, as given in Eq. 4.3.

$$\Delta C/N_0 = 10\, log_{10}\left(\frac{WBW}{NBW}\right) \tag{4.3}$$

where $\Delta C/N_0$ is the gain in aided signal tracking loop threshold in dB.

4.3 Experimental results

To evaluate the performance of proposed dual-frequency signal processing architecture, live satellite signals were collected from block-IIF satellites at GPS L1/L5 frequencies using Javad antenna and Commercial-Off-The-Shelf (COTS) wide-band RF front-end SDRNav40. The received multi-band RF signals are down-converted to a finite IF and digitized at 27.456 MHz sampling frequency. The digitized complex IF data is processed using a dual-frequency software receiver developed for this research project. The details of the tracking loop settings used in the dual-frequency software receiver are given in [P2].

A scatter plot of the position error in the X and Y coordinates computed for a static antenna using L1/L5 ionosphere-free pseudorange observations at an epoch interval of 500 ms over a period of 200 s is shown in Fig. 4.3. The position results computed from signal observations of five visible satellites with HDOP of 2.5. The 1-sigma position error using L1/L5 ionosphere-free pseudorange observations is about 0.8 m, which is reduced to 0.4 m using the common Doppler estimate based two-frequency signal tracking loop. Additionally, carrier smoothing of pseudorange observations using carrier Doppler observations has enhanced the location precision to 0.2 m as shown in Fig. 4.3. It is to be noted that – in the future with an improved geometry of block IIF constellation, and reduced DOP value, there will be twice the decrease in the position accuracy error using L1/L5 signal observations compared to the one shown in Fig. 4.3.

4.4 Summary

The summary of the discussions about the proposed dual-frequency signal processing architecture presented in this chapter are as follows:

- The proposed dual-frequency signal processing architecture is based on the inherent linear relation in the code and carrier frequencies of multi-frequency signals generated

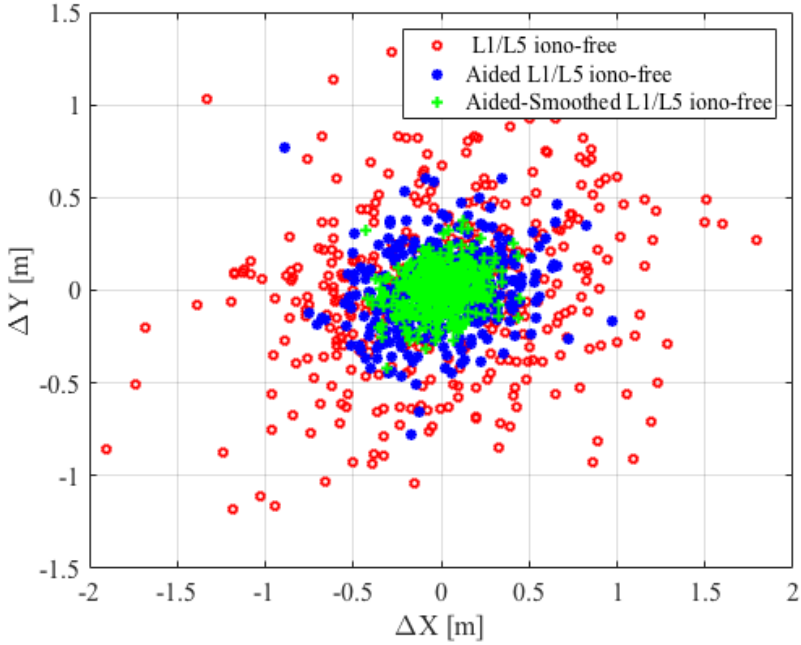

Figure 4.3: Position error using L1/L5 ionosphere-free pseudoranges

from the same the satellite. In the case of GPS L1/L5 and GALILEO E1/E5 signal combination, the higher power L5/E5 signal with pilot channel tracking always outperforms the L1/E1 signal tracking, except in ionosphere-scintillation condition as discussed in Chapter 3. To get benefit of the combined signal observation solution in position accuracy, it is necessary to improve the L1/E1 signal tracking loop performance by taking advantage of the L5/E5 signal. The L5/E5 signal Doppler-aid to L1/E1 signal tracking loop enhances the C/N_0 tracking threshold, which is also demonstrated in [P2]. As a result, the L1/E1 signal tracking loop threshold is improved to be on par with the L5/E5 tracking loop threshold. The L5/E5 Doppler-aided L1/L5 and E1/E5 dual-frequency signal tracking loop performance is determined by the higher performance aiding signal, L5/E5.

- The two-frequency signals tracked using common Doppler observation tend to have correlated observation errors. These correlated observation errors indeed cancel out in the linear combination of observations, i.e. ionosphere-free, wide-lane etc. As a result, the signal observation accuracy and precision improves. Furthermore, the carrier Doppler smoothing of code pseudorange observation will improve the precision of position solution.

- In conclusion, the common Doppler-aided two-frequency signal tracking and then code pseudorange observation smoothing using carrier Doppler observations has improved the overall dual-frequency receiver signal tracking sensitivity, observation accuracy, precision, and robustness to interference. The experimental results using GPS L1/L5 signals have shown that the position error is reduced to 50%. The combined signal C/N_0 tracking threshold is improved to that of the higher performance L5 channel [P2].

5 Adaptive Multi-frequency GNSS Signal Tracking Algorithms

To adapt to the changes in modernized GNSS infrastructure, the future GNSS receiver has to be enabled to process multiple frequency channels from multiple GNSS systems. However, the processing of such a large number of frequency channels is quite challenging and computationally expensive to the GNSS receiver. There is a dire necessity for the development of novel signal processing techniques to improve the computational efficiency and to extract the performance benefits of multi-frequency signals in GNSS receiver. To take advantage of the diversity in the performance of multi-frequency GNSS signals, a computationally efficient and adaptive multi-frequency GNSS signal tracking architecture is proposed in [P3] and [P5].

This chapter presents the details of the proposed centralized dynamics multi-frequency carrier tracking architecture. The contributions of [P3] and [P5] are as follows:

- Overview of the proposed centralized dynamics multi-frequency signal tracking loop architecture [P3] based on the configuration of the single-frequency carrier tracking loop discussed in this chapter.
- Realization of the centralized dynamics tracking loop filter using an AKF, to enable adaptive tracking loop Bandwidth (BW) in response to varying signal conditions.
- Presentation of the criteria for measurement model switching in AKF to adapt to the changing signal conditions.
- Demonstration of the operation of an adaptive centralized dynamics multi-frequency carrier tracking loop in response to the changing signal dynamics and power levels.

To build the basis for the development of a centralized dynamics multi-frequency carrier tracking loop, a review of the single-frequency carrier tracking loop is presented in the following section.

5.1 Single-frequency carrier tracking loop

The received GNSS signal carrier-phase variations are subjected to both high-frequency LOS signal dynamics and low-frequency signal dynamics due to ionospheric TEC variations and reference clock drift as discussed in Chapter 2. Based on this information, a scalar carrier tracking loop can be configured as a combination of a high-dynamics tracking loop and a low-dynamics tracking loop as shown in Fig. 5.1. The carrier-phase discriminator

(PD) computes the phase error between the received and reference signal. The output of the PD, z_k, is processed by both a low-dynamics tracking narrow-band filter and a higher order wide-band filter simultaneously. The narrow-band filter is designed to estimate the low-frequency component of the carrier-phase variations, $\hat{z}_k$, while the wide-band loop filter estimates the high-frequency component of phase variations, $\hat{f}_{GD_k}$. Finally, the sum of the LOS geometric Doppler shift estimated by the wide-band filter and the residual phase and frequency error estimated by the narrow loop filter, $\delta\hat{\phi}_k$, are used to synchronize the carrier NCO with the received signal phase variations. However, this configuration has no additional benefit in improving signal tracking threshold, because the effective measurement processing BW is the same as that of a single wide-band tracking loop. In a way, the carrier tracking loop threshold can be improved using a narrow-band tracking loop with external Doppler aiding [54], [14]. The LOS Doppler aid, $\hat{f}_{GD_k}$, to the carrier tracking loop can be provided by the navigation filter using VTL or external Doppler aid from the velocity sensors.

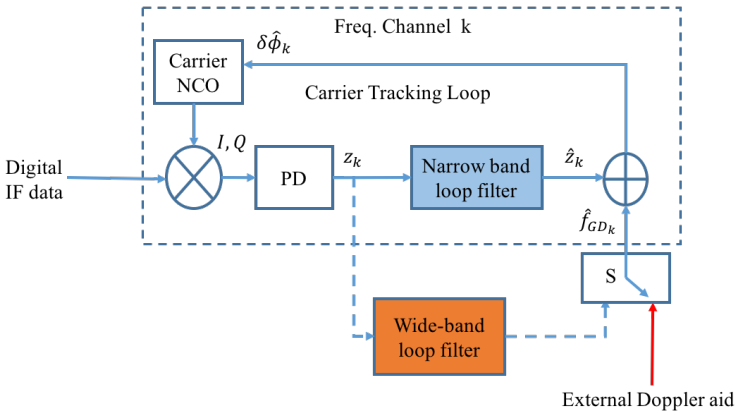

Figure 5.1: Scalar carrier tracking loop

The single-frequency channel carrier tracking loop configuration illustrated in Fig. 5.1 can be extended to multiple frequency channels as discussed in the following section.

5.2 Multi-frequency carrier tracking loop

In a multi-frequency GNSS receiver, each frequency channel carrier tracking loop is configured as a combination of the low-dynamics signal tracking loop and high-dynamics signal tracking loop as shown in Fig. 5.2. The wide-band loop filter in each frequency channel is used to estimate the signal phase variations due to LOS dynamics, while the narrow-band PLL in each channel estimates the residual phase variations specific to each frequency signal.

The LOS geometric Doppler shift which is common to multiple frequency channels can be estimated by the aiding from external inertial sensors or from the navigation filter using VTL or from the co-existing frequency channels. Among all these alternatives, the most beneficial way is to make use of the co-existing frequency channel phase measurements to estimate the LOS geometric Doppler shift, as shown in [P3]. To improve the computational efficiency of the multi-frequency signal tracking process, the wide-band filter in each frequency channel can be replaced by one common high-dynamics tracking loop filter to

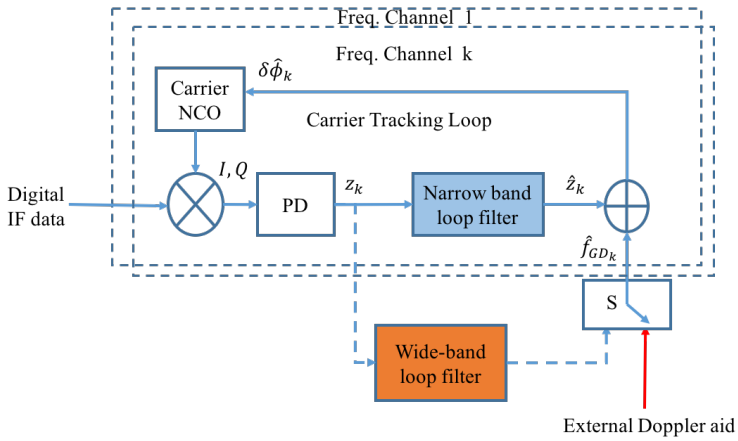

Figure 5.2: Multi-frequency carrier tracking loop

estimate the LOS signal phase variations and then aid all the channels with appropriate scaling, which is discussed in the following section.

5.3 Centralized dynamics multi-frequency GNSS carrier tracking

The idea of the centralized dynamics multi-frequency carrier tracking loop architecture is based on the fact that LOS dynamics are common to multiple frequency signals received from the same satellite as shown in Eq. 2.10. This common signal dynamics information can be estimated by means of a centralized wide-band loop filter, then, the effort to track them with individual frequency channel PLLs can be reduced. Hence, a single centralized wide-band filter is employed to track the common carrier-phase variations and also to improve the computational efficiency in multiple frequency signals tracking as shown in Fig. 5.3. Additionally, the closed loop PLL with a narrow BW filter is essential in each frequency channel to track any residual phase variations specific to each channel. An appropriate loop BW to use in the PLL of each frequency channel can be obtained from a prior estimation of the residual phase error. The carrier-aided code tracking loop is employed to synchronize the local signal code-phase with the received signal code-phase variations in each frequency channel.

The centralized dynamics tracking loop filter (CTL) estimates the common LOS geometric Doppler frequency using a combination of carrier-phase error measurements from high C/N_0 frequency channels by sensing the channel condition. The CTL provides geometric Doppler aid to the narrow BW PLL in each frequency channel. The residual phase and frequency variations specific to each frequency channel will be tracked by narrow BW PLL. The sum of the geometric Doppler frequency estimate aided by CTL and the residual phase and frequency estimated by a narrow BW PLL will be used to tune the carrier NCO in each frequency channel,

$$\begin{aligned} \delta\hat{\phi}_k &= \hat{z}_k + \delta\hat{f}_{GD_k} \quad [\text{Hz}] \\ \hat{z}_k &= \delta\hat{\phi}_0 + \delta\hat{f}_{RD_k} \quad [\text{Hz}] \end{aligned} \tag{5.1}$$

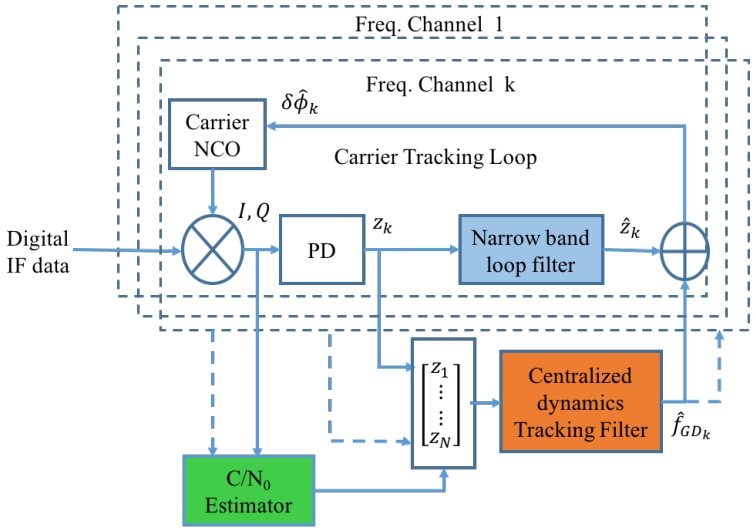

Figure 5.3: Centralized dynamics multi-frequency tracking loop architecture

where $\delta\hat{\phi}_k$ is the total control input to carrier oscillator; $\hat{z}_k$ is the estimate of filtered residual phase, $\delta\hat{\phi}_0$, and frequency error $\delta\hat{f}_{RD_k}$ due to frequency dependent error sources in the subscripted frequency channel; $\delta\hat{f}_{GD_k}$ is the geometric Doppler shift in frequency estimated by the CTL.

The CTL can be realized using a conventional higher-order fixed BW loop filter to follow the expected signal dynamics in a known signal environment as discussed in [P4]. Since the LOS signal phase variations due to relative movement between the satellite and receiver are significantly higher than the residual phase variations due to other sources, the BW of the common dynamic tracking filter is wider and of a higher order than the narrow-band filters in each channel. Typically, third-order PLL has a BW of about 15 Hz for CTL and a second-order PLL has a loop BW of about 2 Hz for individual loops employed in case of a static receiver.

For efficient tracking loop operation in unknown time-varying signal environments, it is necessary to design an adaptive tracking loop-filter. The adaptation can be done according to C/N_0 and the changing signal dynamics. There are many approaches to realize an adaptive tracking loop with respect to the changing signal environment, as discussed in [71]. The AKF is considered here as a suitable algorithm to enable an optimal adaptive carrier tracking loop BW [72]. The CTL architecture realized using an AKF is discussed in the following section.

5.4 Centralized dynamics multi-frequency carrier tracking via AKF

The Kalman filter is chosen to effectively blend multiple frequency channel carrier-phase observations and to track common LOS signal dynamics of the received multiple frequency signals. The signal-tracking KF is regarded as identical to the Digital Phase Lock Loop (DPLL) with time-varying noise BW that optimally enhances the receiver tracking performance in response to the user signal environments [73], [74]. Several

state-space formulations to design a KF-based signal tracking exist, depending on the measurement variables and the state to be estimated. The measurement vector in the carrier tracking loop can be defined either from the complex correlator output or from the phase discriminator output. In the current research, the phase discriminator outputs are used as measurements, to make use of the conventional tracking loop measurements. The limitation of this approach is that the measurement noise is no longer an Additive White Gaussian Noise (AWGN). The nonlinear phase discriminator function causes the loss of the AWGN properties if the phase error is beyond the linear region of discriminator. In the proposed multi-frequency signal dynamics tracking loop architecture, the KF is replacing the F-PLL loop filter in conventional architectures in order to estimate the common carrier-phase error variation between the received and reference signals, based on the multiple-frequency signal phase and frequency error measurements.

The criteria to choose the carrier-phase and frequency error measurements from multiple frequency channels in a time-varying signal environment are discussed in the following section.

5.4.1 Multi-frequency channel measurement processing

In a real GNSS signal environment, multiple frequency signals are subject to frequency selective interference either at the same time (concurrent) or at different time instants (non-concurrent). For an efficient tracking loop operation in such an interference scenario, carrier-phase and frequency error measurements from multiple frequency channels can be processed in two different ways within the centralized carrier dynamics tracking KF. Namely,

1. **Concurrent** frequency selective interference occurs in urban canyon and indoors, where the satellite will be shadowed for a short duration, that causes all frequency signals to be attenuated or blocked at the same time. In this case, it is beneficial to combine multiple frequency channel measurements in an optimal way to obtain a Minimum Mean Square Error (MMSE) estimate of the common geometric Doppler frequency error between the received and reference signals [26]. This approach will reduce the influence of interference in each frequency channel measurement by means of a KF gain distribution. The measurement vector, $\mathbf{z}$, in this case, can be represented as a vector of measurements from N multiple frequency channels,

$$\mathbf{z} = \left[\ \mathbf{z}_1, \cdots, \mathbf{z}_N \ \right], \tag{5.2}$$

   This approach has limitations to be used in non-concurrent interference scenarios, due to the propagation of errors from weak signal tracking loops to strong signal tracking loops.

2. **Non-concurrent** frequency selective interference is most likely due to intentional or unintentional RF interference such as multipath, jamming, and spoofing. In such signal conditions, it is beneficial to use measurements from a signal frequency channel that is not under the influence of interference. This approach avoids the propagation of errors from weak signal tracking channels to stronger signal tracking channels. In a non-concurrent interference signal scenario, the measurement vector is chosen from multiple frequency channels based on a maximum C/N_0 criteria,

$$\mathbf{z} = \max_{C/N_0} \left[\mathbf{z}_1, \cdots, \mathbf{z}_N \right]. \tag{5.3}$$

Notice that this approach is not a suitable solution when all the frequency channels are under the influence of interference.

The two signal conditions discussed above will be sensed by using C/N_0 estimator in each frequency channel, compared to the C/N_0 threshold. In the former case, the optimal value KF gain for weighting each frequency channel measurement is computed based on the measurement noise variance. In the latter case, frequency channel measurements with a high C/N_0 will be chosen to estimate the KF error-state vector.

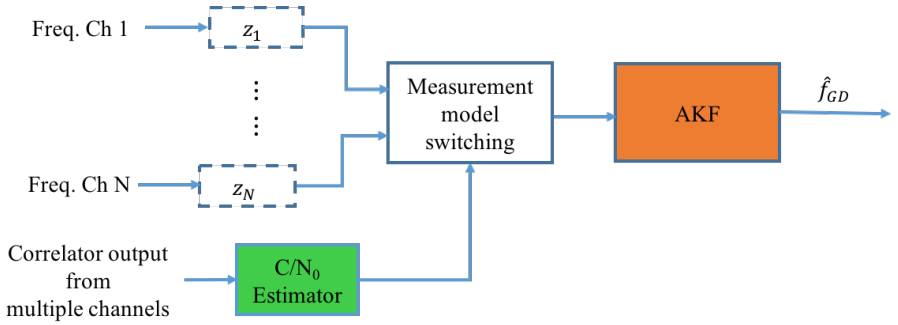

Figure 5.4: Geometric Doppler frequency estimation using an Adaptive Kalman Filter scheme.

It is to be noted that received signals with C/N_0 below 30 dB-Hz are considered as weak signals, while signal in the C/N_0 above 30 dB-Hz are considered as stronger signals [21]. Hence, the measurement model switching in KF is based on the C/N_0 threshold of 30 dB-Hz. To avoid the propagation of errors from weak signal channel measurements to stronger channel measurements, it is necessary to sense and exclude the weak signal channel measurements from the measurement vector. The channel condition is indicated by the C/N_0 estimator to measurement switching block, in order to switch between concurrent and non-concurrent measurement models as shown in Fig. 5.4.

The state and measurement dynamic models of the Kalman filter are discussed in the following section.

5.4.2 Kalman filter state and measurement dynamic models

The linear state dynamic model for the error-state KF can be written as,

$$\delta \mathbf{x}_{t+1} = \mathbf{F}\delta \mathbf{x}_t + \Gamma w_t \tag{5.4}$$

where $\delta \mathbf{x}_t$ is the $n \times 1$ error-state vector at epoch t; $\mathbf{F}$ is the $n \times n$ non-singular state transition matrix from epoch t to $t+1$; Γ is the $n \times 1$ noise gain vector; w_t is the zero mean additive white Gaussian process noise sequence with variance $\sigma^2_{w_t}$.

The state dynamic model in the centralized multi-frequency signal dynamics tracking Kalman Filter (KF) is assumed to be a discrete Wiener process acceleration model [52] to bear jerk type of dynamics. The states of the KF are carrier-phase error, frequency error and frequency rate error. The error-state dynamic model can be transformed to

range domain by scaling with the wavelength as,

$$\begin{bmatrix} \delta\phi_k \\ \delta f_{D_k} \\ \delta \dot{f}_{D_k} \end{bmatrix}_{t+1} \lambda_k = \begin{bmatrix} 1 & T & \frac{T^2}{2} \\ 0 & 1 & T \\ 0 & 0 & 1 \end{bmatrix} \begin{bmatrix} \delta\phi_k \\ \delta f_{D_k} \\ \delta \dot{f}_{D_k} \end{bmatrix}_t \lambda_k + \begin{bmatrix} \frac{T^2}{2} \\ T \\ 1 \end{bmatrix} w_t \lambda_k, \tag{5.5}$$

The KF error-state vector can be written in the range domain as,

$$\begin{bmatrix} \delta\rho \\ \delta\dot{\rho} \\ \delta\ddot{\rho} \end{bmatrix}_{t+1} = \begin{bmatrix} 1 & T & \frac{T^2}{2} \\ 0 & 1 & T \\ 0 & 0 & 1 \end{bmatrix} \begin{bmatrix} \delta\rho \\ \delta\dot{\rho} \\ \delta\ddot{\rho} \end{bmatrix}_t + \begin{bmatrix} \frac{T^2}{2} \\ T \\ 1 \end{bmatrix} w_t \lambda_k, \tag{5.6}$$

In this model, the white noise process w_t represents the acceleration increment over the sampling period. The covariance of the process noise multiplied by the gain, Γw_t, is

$$\mathbf{Q}_t = \Gamma \sigma_{w_t}^2 \Gamma^\top = \begin{bmatrix} \frac{T^4}{2} & \frac{T^3}{2} & \frac{T^2}{2} \\ \frac{T^3}{2} & T^2 & T \\ \frac{T^2}{2} & T & 1 \end{bmatrix} q_t \tag{5.7}$$

where $q_t = \sigma_{w_t}^2$ is the process noise acceleration variance in m^2/s^4. For this model, the practical range of σ_{w_t} should be of the order of maximum acceleration increment over the sampling period.

The measurement dynamic model related to the error state vector can be represented as

$$\mathbf{z}_t = \mathbf{H}\delta\mathbf{x}_t + \mathbf{n}_t, \tag{5.8}$$

$\mathbf{z}_t$ is the $m \times 1$ measurement vector at epoch t; $\mathbf{H}$ is the $m \times n$ measurement design matrix; $\mathbf{n}_t$ is zero mean Gaussian measurement noise sequence with covariance, $\mathbf{R}_t$. The single-frequency channel carrier-phase and frequency measurements related to the error-state vector in the range domain can be written as,

$$\begin{bmatrix} \lambda_k e_{\phi_k} \\ \lambda_k e_{f_k} \end{bmatrix}_t = \begin{bmatrix} 1 & 0 & 0 \\ 0 & 1 & 0 \end{bmatrix} \begin{bmatrix} \delta\rho \\ \delta\dot{\rho} \\ \delta\ddot{\rho} \end{bmatrix}_t + \begin{bmatrix} n_{\phi_k} \\ n_{f_k} \end{bmatrix} \lambda_k. \tag{5.9}$$

For a single-frequency channel tracking, $\mathbf{R}_t$ is a 2×2 matrix. $\mathbf{Q}_t$ and $\mathbf{R}_t$ are positive definite matrices (i.e. $\mathbf{Q} \succ 0$, $\mathbf{R} \succ 0$).

The KF requires an initialization of the state vector, $\delta\mathbf{x}_0$, and state error covariance $\mathbf{P}_0$, and an exact knowledge of the process noise covariance $\mathbf{Q}_t$ and measurement noise covariance $\mathbf{R}_t$, based on the prior information of the system and signal operating environment. The steady-state KF gain can be computed as [75],

$$\mathbf{K}_{t+1} = \mathbf{P}_{t+1|t}\mathbf{H}^T(\mathbf{H}\mathbf{P}_{t+1|t}\mathbf{H}^T + \mathbf{R}_{t+1})^{-1}, \tag{5.10}$$

$$\mathbf{P}_{t+1|t} = \mathbf{F}\mathbf{P}_{t|t}\mathbf{F}^T + \mathbf{Q}_t, \tag{5.11}$$

where $\mathbf{K}_{t+1}$ is the 3×2 Kalman gain matrix at epoch $t+1$.

The error-state KF equations can be written as

$$\delta\hat{\mathbf{x}}_{t+1|t} = \mathbf{F}\delta\hat{\mathbf{x}}_{t|t}, \tag{5.12}$$

$$\delta\hat{\mathbf{x}}_{t+1|t+1} = \delta\hat{\mathbf{x}}_{t+1|t} + \mathbf{K}_{t+1}\tilde{\mathbf{z}}_{t+1}, \tag{5.13}$$

$$\tilde{\mathbf{z}}_{t+1} = \mathbf{z}_{t+1} - \mathbf{H}\delta\hat{\mathbf{x}}_{t+1|t}, \tag{5.14}$$

with $\tilde{\mathbf{z}}_{t+1}$ the innovation of the measurement vector, which is used to update the predicted state vector, $\delta\hat{\mathbf{x}}_{t+1|t}$, and $\mathbf{P}_{t+1|t}$ is the prediction error covariance matrix.

The multi-frequency signal dynamics tracking KF state-vector can be initialized with a prior estimate of phase and frequency errors, which are estimated within the STL, as,

$$\delta\hat{\mathbf{x}}_0 = \begin{bmatrix} \delta\rho \\ \delta\dot{\rho} \\ \delta\ddot{\rho} \end{bmatrix} = \begin{bmatrix} \delta\phi_k \\ \delta f_{D_k} \\ \delta\dot{f}_{D_k} \end{bmatrix} \lambda_k. \tag{5.15}$$

The KF error-state estimate $\delta\hat{\mathbf{X}}_{t+1}$ is conditioned on knowing the true values of the system parameters $\mathbf{F}, \mathbf{P}, \mathbf{H}, \mathbf{Q}_t$ and $\mathbf{R}_t$. The assumed noise statistics $\mathbf{Q}_t$ and $\mathbf{R}_t$ are not unconditionally valid for GNSS signal tracking in time-varying signal environments such as ionosphere scintillation, blockage and interference. Hence, in the signal tracking KF, the process noise and measurement errors must be estimated from the measurements. This process leads to tuning the KF using statistical estimation of $\mathbf{Q}_t$ and $\mathbf{R}_t$ values based on the measurements. The AKF is a suitable method for dynamically adjusting the parameters of the KF. There are many approaches for tuning the AKF as summarized in [76]. An innovation-based adaptive estimation is used as the most suitable technique in multiple sensor fusion applications [77] and [78], which is used in this research thesis [P5] for common signal dynamics tracking based on the multiple frequency signal carrier-phase error measurements. The idea of an innovation-based AKF is to regularly estimate measurement and process noise covariances using instant carrier-phase error measurements as discussed in the next section.

5.5 Estimation of measurement and process noise covariances

An essential step in the innovation-based AKF is the estimation of the innovation covariance. The covariance of the innovation sequence can be estimated using a simple moving average filter as given in [72],

$$\hat{\mathbf{C}}_{\tilde{\mathbf{z}}_t} = \frac{1}{M} \sum_{j=t-M+1}^{t} \tilde{\mathbf{z}}_j \tilde{\mathbf{z}}_j^T \tag{5.16}$$

where $\tilde{\mathbf{z}}_t$ is the measurement innovation sequence; M is the number of samples in the window.

Alternatively, innovation covariance can be estimated from the measurement noise covariance as,

$$\hat{\mathbf{C}}_{\tilde{\mathbf{z}}_t} = \left[\mathbf{H}\mathbf{P}_{t|t-1}\mathbf{H}^T + \mathbf{R}_t\right] \tag{5.17}$$

The measurement noise variance in GNSS receiver can be obtained from the carrier to noise ratio estimator in each frequency channel carrier tracking loop, as given in [48],

$$\sigma^2_{e_{\phi_k}} = \left(\frac{1}{4\pi^2(C/N_0)_k T)}\right)\left(1 + \frac{1}{2\pi(C/N_0)_k T}\right) \quad [cycles^2] \tag{5.18}$$

$$\sigma^2_{e_{f_k}} = \frac{2\sigma^2_{e_{\phi_k}}}{T^2} \quad [cycles^2/sec^2] \tag{5.19}$$

The details of the carrier-to-noise ratio estimation techniques in GNSS receiver can found in [79].

The measurement noise covariance matrix for N independent multiple frequency channel carrier-phase and frequency error measurements can be represented as a diagonal matrix, $\hat{\mathbf{R}}_t = \text{diag}(\sigma^2_{e_{\phi_1}}, \sigma^2_{e_{f_1}}, \cdots, \sigma^2_{e_{\phi_N}}, \sigma^2_{e_{f_N}})$.

Similarly, the signal dynamics information represented by the process noise covariance $\mathbf{Q_t}$ can be obtained using Doppler frequency rate measurements $\dot{f}_{D_k}$ in each frequency channel. A simple phase acceleration process noise variance estimation using a moving average estimator within a specified window is [80],

$$q_t = \frac{1}{M-1} \sum_{j=t-M+1}^{t} \left[\dot{f}_{D_k}(j) - \frac{1}{M} \sum_{j=t-M+1}^{t} \left[\dot{f}_{D_k}(j) \right] \right]^2 \tag{5.20}$$

where the units of q_t are [cyc^2/s^4]; $\dot{f}_{D_k}(j)$ is the signal phase acceleration measurement in [cyc/s^2] obtained from the difference of consequent Doppler frequency outputs in the signal carrier tracking loop. The process noise covariance $\mathbf{Q}_t$ can be estimated by substituting q_t in Eq. 5.7. The estimated values of $\mathbf{R}_t$ and $\mathbf{Q}_t$ can be used to calculate the time-varying optimal value of the KF gain in response to received signal power level and dynamics.

However, the simultaneous update of $\mathbf{R}_t$ and $\mathbf{Q}_t$ is not a viable solution as they negatively affect the filter response. Hence, it is reasonable to estimate and update the measurement noise and process noise covariance alternatively in the Kalman gain estimation [76]. The Kalman filter gain adaption to the alternative estimation of signal measurement noise variance and process noise variance is demonstrated in the following section

5.6 Kalman filter gain adaption to measurement error variance and signal dynamics

In centralized dynamics tracking loop filter, carrier-phase discriminator output measurements from multiple frequency channels will be combined statistically in an optimal way to obtain the best possible estimate of $\delta\mathbf{x}_t$ based on the time-varying estimates of $\mathbf{Q}_t, \mathbf{R}_t$ and $\mathbf{K}_t$ values. The process noise covariance $\mathbf{Q}_t$ represents the rate of change of the state, while the measurement noise covariance $\mathbf{R}_t$ represents the accuracy of the signal measurements. The optimal weight to multiple signal carrier-phase measurements depends on individual signal measurement noise variance $\mathbf{R}_t$ and manifestation of the KF gain. The Kalman gain can be represented in terms of estimated innovation covariance and $\mathbf{Q}_t$ as,

$$\mathbf{K}_t = (\mathbf{F}\mathbf{P}_{t|t-1}\mathbf{F}^T + \mathbf{Q}_t)\mathbf{H}^T \hat{\mathbf{C}}^{-1}_{\tilde{\mathbf{z}}_t}. \tag{5.21}$$

Then, the KF gain will be manifested based on the carrier-phase measurement noise variance and signal Doppler rate as discussed earlier.

The KF equivalent noise BW is characterized in comparison to the conventional PLL loop filter in [81], [82]. The steady-state KF equivalent noise BW can be computed from the Kalman gain, which is a function of tuning parameters $\mathbf{Q_t}$ and $\mathbf{R_t}$ as given in [80],

$$B_{eq} = \frac{(\mathbf{F}\mathbf{P}_{t|t-1}\mathbf{F}^T + \mathbf{Q}_t)\mathbf{H}^T \left[\mathbf{H}\mathbf{P}_{t|t-1}\mathbf{H}^T + \mathbf{R}_t\right]^{-1}}{c_n T} \tag{5.22}$$

where c_n is the filter coefficient for the n-th order PLL and T is the signal integration time.

For a third order loop filter, $c_n = 3.048$ and the steady-state gain matrix $\mathbf{K}$ is directly proportional to $\mathbf{Q_t}$ and inversely proportional to $\mathbf{R_t}$. This relation enables to construct an adaptive filter BW for time-varying signal environments. In weak signal environments, the measurement noise variance $\mathbf{R_t}$ increases, which in turn reduces the Kalman gain. In high-dynamics signal environments, the process noise increases, and as a result the Kalman gain tends to increase proportionally. The Kalman-filter equivalent BW changes proportionally to the variation of the gain in high dynamics and weak signal conditions.

For instance, KF gain and equivalent BW adaptation to the changing signal dynamics and signal C/N_0 levels in two-frequency channels are shown in the Figs. 5.5 and 5.6

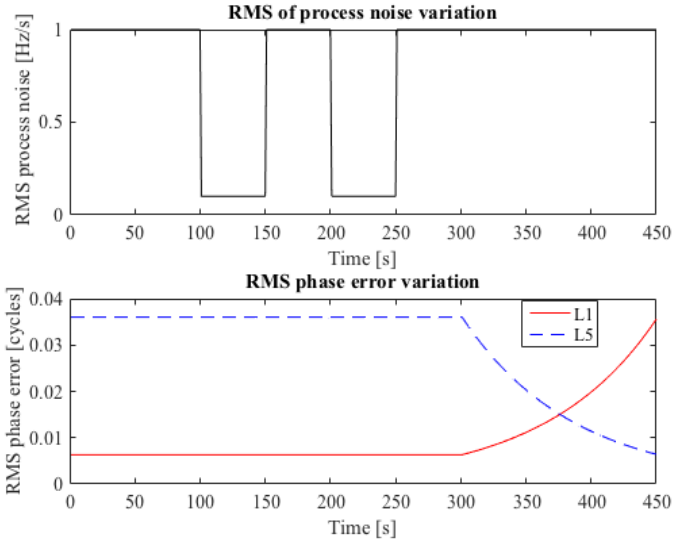

Figure 5.5: Process noise and phase measurement error variation in two-frequency channels

The Root Mean Square (RMS) process noise due to the received signal dynamics is common to two-frequency channels, while the RMS measurement error varies according to the C/N_0 in each RF channel. The time-varying GNSS signal environment is simulated with varying signal dynamics and signal measurement errors to demonstrate the operation of the proposed centralized multi-frequency carrier tracking using two-frequency channel measurements. The RMS process noise value is switching between 1 Hz/s and 0.1 Hz/s, while the carrier-phase error in two frequency channels is varying continuously as shown in Fig. 5.5. The KF gain and equivalent BW are optimally adjusted to the changing signal dynamics and measurement noise variance in two-frequency channels as shown in Fig. 5.6.

5.7 Summary

The summary of the discussions in this chapter about the contributions of research publications in [P3] and [P5] are presented in this section.

- To enable the multiple frequency channels to complement each other in signal tracking process, a centralized dynamics multi-frequency tracking loop architecture

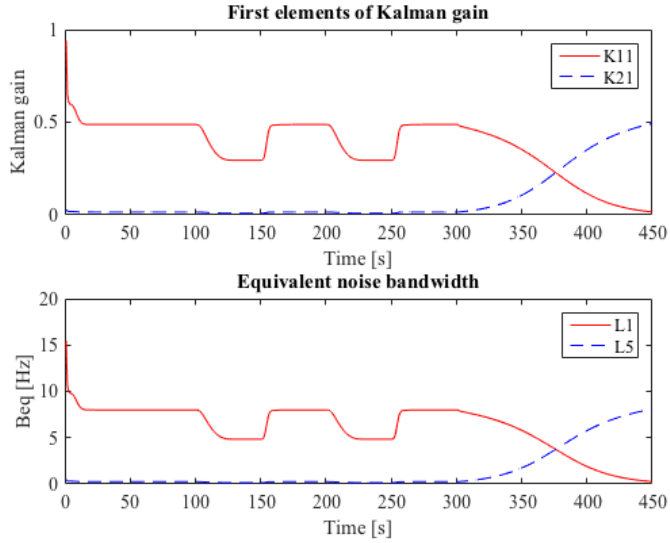

Figure 5.6: Kalman gain adaption to two-frequency channel measurements

is proposed in [P3]. The proposed CTL architecture takes advantage of the coherency is satellite signal generation and diversity in the performance of multiple frequency signals in a time-varying GNSS signal environment. This architecture is realized using a single dynamics tracking loop filter (CTL) and multiple narrow BW PLLs. The CTL estimates the common LOS phase variations, while the narrow-band PLL estimates the residual phase variations specific to each frequency channel. The proposed architecture is computationally efficient and tends to enhance the individual signal tracking sensitivity and robustness to RF interference.

- For an efficient multi-frequency channel tracking loop operation in a time-varying signal environment, the CTL is realized using an adaptive Kalman filter to enable adaptive tracking loop BW in response to the received signal power level and dynamics [P5].

- The operation of the proposed CTL architecture is shown in Section 5.6 using two-frequency channel carrier-phase measurements in varying signal conditions. Furthermore, the performance of this architecture is evaluated using live satellite signals collected over multiple frequency channels from block-IIF satellites in [P3]. The robustness of the CTL is tested by subjecting it to matched spectrum jamming signals generated using record and replay procedure in [P5].

6 Performance Benefits of Centralized Dynamics Multi-frequency Tracking Loop

This chapter evaluates the performance benefits of the proposed centralized dynamics tracking loop architecture introduced in Section 5.4 [P5].

6.1 Evaluation of the performance benefits of CTL

To evaluate the performance benefits of the proposed adaptive CTL tracking loop, a simple analysis of KF equivalent BW using single and two-frequency signal measurements is shown with reference to standard PLL fixed loop BW in Fig 6.1. The Kalman filter equivalent BW is computed according to Eq. 5.22 [80] for three different signal dynamics profiles represented by process noise variance, $q = 0.1, 1$ and 10 (cyc^2/s^4) at an assumed C/N_0 of 50 dB-Hz in each frequency channel.

In CTL, either a single or combination of multiple frequency channel phase measurements is utilized to estimate the signal dynamics using AKF. In AKF, the time-varying KF gain and the equivalent BW are adapted to the changing signal dynamics and to the measurement noise sequentially as discussed in Section 5.6. The KF gain coefficients are distributed to give weight to measurements from each channel proportional to the measurement noise statistics.

In frequency-selective interference scenario, where one or more number of frequency channels are under the influence of interference, combining multiple frequency channel measurements causes the propagation of errors from weak signal channels to the strong signal channel tracking loop. In such a case, it is beneficial to use the relatively stronger signal channel measurements to estimate the LOS signal dynamics. In case of concurrent interference scenario, where all the frequency channels are under the influence of fading or attenuation, it is beneficial to use the optimal weighted combination of multiple frequency channel measurements to estimate LOS signal dynamics. In the concurrent interference, Kalman filter gain is distributed to give appropriate weights to all the available frequency channel measurements based on respective signal measurement noise statistics. The equivalent noise BW in each frequency channel tracking loop is adapted proportionally to the Kalman gain distribution across multiple channel measurements. The reduced tracking loop BW in each frequency channel improves C/N_0 tracking threshold. The improved C/N_0 tracking threshold, in turn, increases the signal tracking loop tolerance to RF interference [54]. As a result, the influence of interference on each frequency channel reduces proportionally to the KF BW.

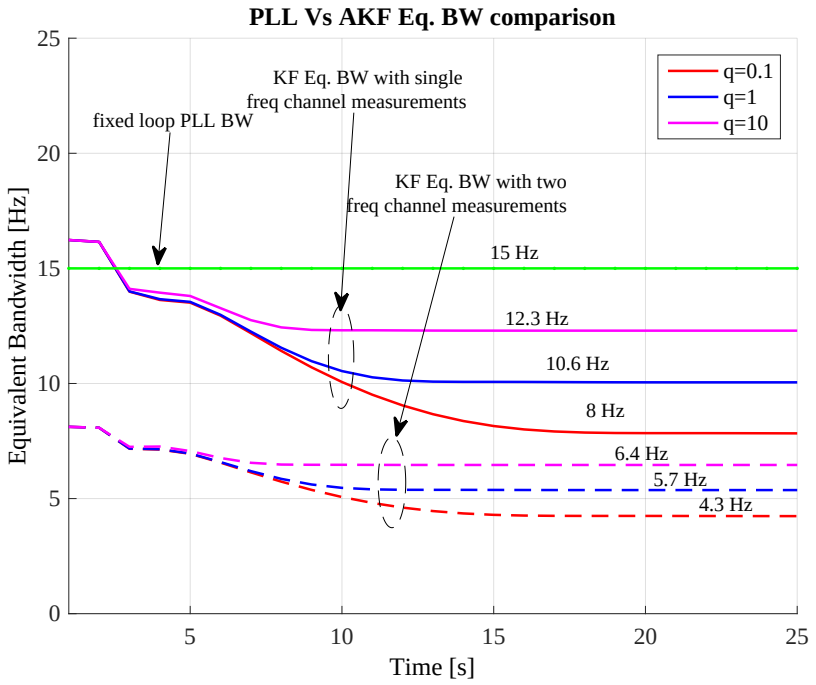

Figure 6.1: Comparison of equivalent BW in fixed BW PLL loop filter and AKF using single and two frequency channel measurements at C/N_0 of 50 dB-Hz

As an example, 1-sigma value of carrier-phase noise in GPS L1 and L5 signal tracking loop using AKF with single and dual-frequency channel measurements is evaluated using analytical error models [48], as shown in Fig. 6.2, at $q = 1$ (cyc^2/s^4).

The steady-state value of the KF equivalent BW using single and dual-frequency channel measurements is 10 Hz and 6 Hz respectively at a process noise variance of $q = 1$ (cyc^2/s^4), as shown in Fig. 6.1. The single frequency channel KF tracking loop of 10 Hz equivalent BW has the benefit of 2 dB tracking threshold. While the dual-channel KF loop of 6 Hz equivalent BW has a benefit of 4 dB tracking threshold in each channel in comparison to the 15 Hz fixed loop BW PLL. The cases of frequency selective interference signal scenario, where the signal dynamics are estimated using a relatively stronger channel phase measurements and all the other frequency channels tracked using second-order PLL of 2 Hz BW, have a benefit of 8 dB improvement in C/N_0 tracking threshold. In conclusion, the narrow loop BW signal tracking using signal dynamics aided from CTL increases the robustness to intentional and unintentional interference in each frequency channel.

The multiple frequency signals transmitted at different radio frequency in the L-band spectrum are influenced differently by the RF interference. A characterization of GPS receiver performance for multi-frequency GNSS signals is shown in Chapter 3. The GPS L5 and GALILEO E5a/E5b signals with 10 times higher chip rate and higher received power have the benefit of more immunity to RF interference than other frequency signals in GPS and GALILEO systems. The GPS L1/GALILEO E1 signals transmitted at higher

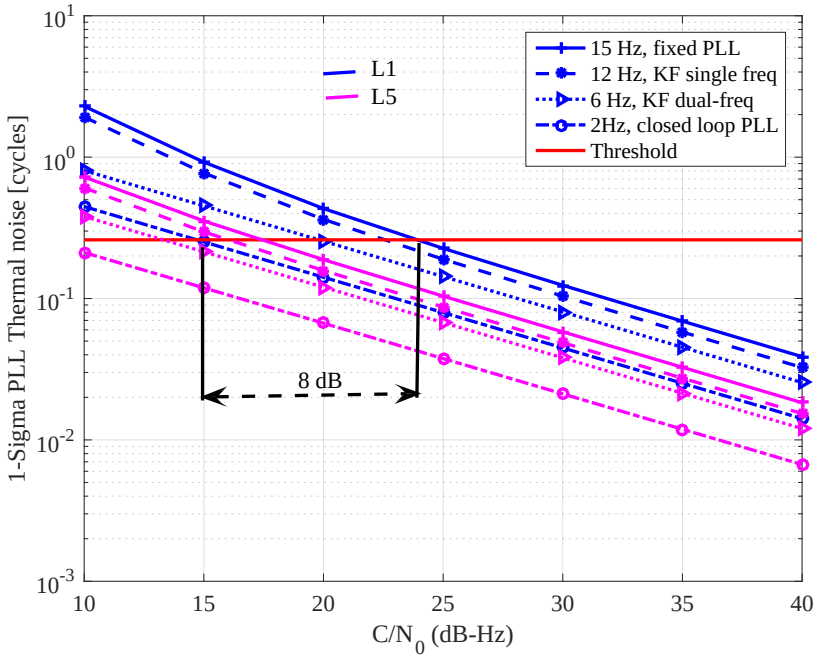

Figure 6.2: Phase error in L1 and L5 signal carrier tracking loop at q=1, using KF with single and dual frequency signal phase observations in reference to fixed loop BW PLL.

RF frequency are more robust to ionosphere scintillation than other signals in GPS and GALILEO systems. Therefore, a suitable collaboration in multi-frequency signal tracking using CTL will enable the multiple frequency signals to complement each other to improve individual signal tracking loop performance in challenging signal environment such as blocking, jamming/spoofing and ionosphere scintillation.

6.2 Summary

The performance benefits of the centralized dynamics multi-frequency GNSS signal tracking loop architecture are summarized in this section.

- **Computational efficiency**

  The replacement of a multiple number of higher order carrier tracking loops by a single centralized dynamics tracking filter and multiple narrow BW PLLs improves the computational efficiency of the GNSS receiver significantly [P3], which in turn is a power-efficient solution.

- **Restoration of temporary loss-of-lock in tracking loop**

  During the receiver operation in real GNSS signal environment, the signal tracking loop may lose lock for a short time interval when the frequency channel is being shadowed or blocked. In such a case, it is necessary to reacquire the signal to resume signal tracking process after the signal reappears. The signal re-acquisition

is a computationally intensive process in scalar tracking loops. In the proposed centralized dynamics multi-frequency tracking architecture, a common geometric Doppler shift aid is provided by the CTL to all the frequency channels, including the blocked channels to restore the lost tracking process after the signal reappears. This, in turn, eliminates the need of re-acquisition process.

- **Robustness to RF interference**

  In multi-frequency CTL architecture, each frequency channel is tracked using narrow BW tracking loop aided by a geometric Doppler estimate from CTL. The narrow band signal tracking improves the signal tracking threshold. The improved signal tracking threshold, in turn, improves the J/S performance of the receiver [54]. Hence, the CTL tracking loop is inherently more immune to RF interference compared to the scalar tracking loop. Also, frequency selective jamming or spoofing on CTL requires higher J/S compared to that of STL to disrupt the intended frequency channel.

- **Robustness to spoofing**

  The CTL provides the LOS signal dynamics aid to the narrow-band tracking loop in each frequency channel. The influence of a spoofing signal with dynamics deviated from the authentic signal on selective frequency channels can be detected and rejected due to the mismatch between the received spoofing signal dynamics and authentic signal dynamics aided by the CTL, $\delta\hat{f}_{GD}$. At most, the frequency selective spoofing impairs the targeted frequency channel from tracking the legitimate signal and leads to a jammed state. Therefore, the false signal can never be tracked by any of the spoofed channels while the authentic signal dynamics are provided by the CTL. Hence, the CTL architecture improves the receiver robustness to frequency selective spoofing by making use of redundancy of a number of frequency signals [P3].

- **Improvement in observation accuracy**

  The common Doppler-aided multi-frequency channel tracking using CTL will result in common mode observation errors in multiple channels. The common-mode observations errors tend to cancel out when a linear combination of the observations are generated, such as ionosphere-free, wide-lane etc. as shown in [P1]. This, in turn, leads to improvement in pseudorange observation accuracy and precision.

- **Improvement in receiver performance**

  The proposed adaptive CTL signal tracking architecture employed in GNSS receiver enables the collaborative and efficient multi-frequency signal tracking operation in a time-varying signal environment. This allows multiple frequency channels to complement each other in challenging signal conditions such as ionosphere scintillation, blockage, fading, jamming, and spoofing. As a result, the overall receiver performance is improved in terms of signal tracking sensitivity, observation accuracy, precision and robustness to interference.

7 Conclusion

This research thesis has studied and analyzed the characteristics of multi-frequency GNSS signals in varying signal conditions. The multi-frequency GNSS signals are like multiple sensors providing the pseudorange and range-rate observations between the satellite and receiver. Each of these signals has different performance capabilities in providing observations at the receiver according to their signal characteristics and channel effects. However, the diversity of the signal characteristics and redundancy of multiple frequency signals can be best utilized to complement each other during signal processing at the receiver. The benefits of multi-frequency GNSS signals can be extracted by employing suitable signal processing algorithms in the receiver, in order to enhance the individual signal tracking sensitivity, observation quality, and reliability of information in time-varying GNSS signal conditions.

Based on the insight of multi-frequency GNSS signal characteristics, this thesis has identified the necessity of collaboration in multi-frequency signal processing at the receiver. The classical signal processing algorithms in GNSS receiver have utilized multi-frequency signal observations to remove common-mode errors in order to improve the observations accuracy. These approaches have limited the utility of multi-frequency signals up to improving the observation accuracy performance by neglecting the other receiver performance parameters. To extract the best performance benefits of multi-frequency GNSS signals, this thesis has proposed the novel centralized dynamics multi-frequency signal tracking architectures to enhance the signal tracking loop performance in time-varying GNSS signal environment. The proposed multi-frequency signal processing algorithms will improve the accuracy and robustness of the position solution. The performance of the proposed multi-frequency signal processing algorithms is tested with the multi-frequency signal processing software developed as part of this research thesis, using the live satellite signals collected from GPS block-IIF satellites. The centralized dynamics multi-frequency signal tracking loop has enhanced the individual channel tracking loop threshold by 7 dB as demonstrated in [P3] and [P5]. The dual-frequency signal processing architecture proposed for the standalone receiver has reduced the position error by 50% [P2].

This chapter summarizes the contributions of this research work presented in Chapters 1- 6 and the publications [P1 - P5] attached to this thesis. Furthermore, some future research ideas are proposed in the area of multi-constellation and multi-frequency GNSS signal processing to provide an improved position solution for a wide range of location-based services.

Chapter 1, presented a brief review of the location-based services, modernization of GNSS infrastructure, and the necessity of the new developments in GNSS receiver design to serve the rapidly changing requirements of civilian GNSS applications. Subsequently, the motivation for the development of novel signal processing techniques to make the

best utilization of multi-frequency GNSS signals to provide improved position solution is discussed. The state-of-the-art research in multi-frequency GNSS signal processing was introduced and the limitations of earlier research work was discussed. In conclusion of this Chapter, the primary objectives and contributions of this research thesis were presented.

Chapter 2, has reviewed the characteristics of multiple frequency signals in each GNSS system. The inherent linear relationship between multiple frequency signals was characterized. The factors that influence the received signal phase variations were discussed. The traditional multi-frequency signal processing architecture was reviewed. The tracking loop design criteria for optimum signal tracking loop operation in varying signal environment was introduced. The summary of Chapter 2, outlined the factors that determine the signal tracking loop threshold.

In Chapter 3, the performance analysis of multi-frequency GNSS receiver using single and combinations of multi-frequency signals was presented. The criteria to select the optimal dual-frequency signal combination for standalone ionosphere-free solution [P1] and integer ambiguity resolution in carrier phase differential positioning was discussed using analytical error models and experimental results as shown in [P4]. The summary of Chapter 3, outlined the limitations of classical multi-frequency signal processing algorithms used to generate linear-combination of observations.

Chapter 4, discussed the common Doppler estimate based two-frequency signal tracking loop architecture proposed and published in [P2]. Two-frequency signal tracking using low noise common Doppler observation had shown the improvement in signal tracking sensitivity and reduced the noise in the linear combination of observations by 50 %. The pseudorange observation smoothing using carrier Doppler observations has enhanced the observation precision. The performance benefits of the proposed dual-frequency signal processing architecture in [P2] was demonstrated using live satellite data collected from block-IIF satellites.

Chapter 5, discussed the contributions of publications in [P3] and [P5]. The inherent linear relationship between multiple frequency signals was characterized and a computationally efficient multi-frequency signal tracking architecture was proposed in [P3] to enhance the individual signal tracking sensitivity and robustness to in-band interference. The proposed approach had shown the improvement in C/N_0 tracking threshold of about 7 dB. The analytical and experimental verification of the proposed CTL tracking loop is shown in [P3]. In time-varying GNSS signal environment, the multiple frequency signals are often subjected to dynamics and intentional or unintentional RF interference. To track multiple frequency signals in such a challenging signal environment, CTL tracking loop proposed in [P3] was realized using an adaptive Kalman filter, as shown in [P5]. The common signal dynamics tracking loop bandwidth is adjusted optimally using Kalman filter gain by sensing the signal environment through estimation of measurement and process noise statistics from the received signal carrier phase measurements. The tracking loop bandwidth adjustment in response to varying signal levels and dynamics improved the signal tracking sensitivity and robustness to interference as demonstrated in [P5].

Chapter 6, evaluated the performance benefits of the proposed adaptive CTL tracking loop architecture in tracking multi-frequency GNSS signals in varying signal conditions.

In conclusion, by employing the advanced signal tracking algorithms proposed in this research thesis, it is possible to extract the best performance benefits of multiple frequency signals in the GNSS receiver. This will enable to overcome the inherent limitations of

the single-frequency solution and enhance the receiver signal tracking sensitivity, position accuracy, precision and robustness to interference.

Future Work: During the developments of the current research work, a number assumptions were made and some issues were not resolved, which can be considered for the future research. A summary of the research ideas which can be realized in future in a short-time frame and in the long-time frame are outlined here.

- **Research scope in short-term time frame**
- The work presented in [P1] and [P4] can be extended to find the optimum combination of two or more frequency signals for many other civilian applications by considering the requirements and using signals from any multi-frequency GNSS system.
- The proposed dual-frequency signal processing algorithms in [P2] can be extended for high dynamic applications by analyzing the differences in code and carrier Doppler estimate in two-frequency channels subjected to dynamic signal conditions.
- The centralized dynamics multi-frequency channel tracking architecture proposed in [P3] is the most suitable solution in a time-varying GNSS signal environment. However, when the satellite is shadowed in the urban-canyon, then all of the multiple frequency signals from that satellite may be attenuated to low C/N_0 level and fail to estimate signal dynamics using CTL. In such signal scenario, it is necessary to receive external Doppler aiding either from the co-existing stronger satellite signals or inertial sensor to enhance the signal tracking performance. Hence, CTL integrated to external Doppler aiding can be tested in future work to analyze the multi-frequency channel tracking loop performance when the satellite is shadowed or blocked.
- **Research scope in long-term time frame**
- The future is all about multi-constellation and multi-frequency signals. Hence, there is a great scope to research on the development of signal processing algorithms to extract the benefits of multi-frequency and multi-system signals in order to provide accurate and reliable position solution to future location-based services.
- Nowadays, considering the necessity of location-based services, the future location information cannot rely on one technology. Hence, there is the necessity of the integration of position technologies such as GNSS, cellular technologies, inertial sensors, cloud processing in IoT, and so on. This opens up the scope of research on the context-based signal processing and positioning algorithms. This is all about sensing the signal environment and then to decide on which signals are suitable to process to compute the position solution.
- Till now the scope of the radio navigation technology is limited to the terrestrial applications. In future, the scope of extending radio navigation technology beyond the terrestrial region such as for interplanetary or navigation on the Moon generates great challenges in position computation, realizing the facts about new environmental effects, path loss, signal delays, and signal dynamics.
- The GNSS signals being a radio navigation signals are vulnerable to intentional and unintentional interference. Moreover, the usage of GNSS based positioning in

safety- and liability-critical applications has drawn the attention of many intentional interfere-rs. The single frequency channel solution was severely limited in mitigating and detecting any intentional interference sources. Now, with more number of signals from multiple systems, there is a scope to detect, mitigate, and even to localize the source of interference. However, robust and efficient interference detection, localization, and mitigation algorithms with multi-frequency and multi-GNSS are still to be developed.

- The GNSS based location solution has the limitations to use in miniaturized battery powered devices such as IoT, due to its high power consumption. To make the GNSS position solution more robust and power efficient, the cloud GNSS is a potential alternative to provide location solution. The cloud GNSS is still in the conceptual stage [83], which needs future research contribution.

Bibliography

[1] EGSA, "GNSS market report," European GNSS Agency, Technical Report Issue 4, 2017.

[2] J. A. Klobuchar, "Ionospheric time-delay algorithms for single-frequency GPS users," *IEEE Transactions on Aerospace and Electronic Systems*, vol. 23, no. 3, pp. 325–331, 1987.

[3] "European GNSS (GALILEO) open service-ionospheric correction algorithm for GALILEO single frequency users," European Union, Technical Report 1.2, 2016.

[4] J. A. Klobuchar, "Total ionosphere effects on GPS," *GPS World*, 1991.

[5] R. Píriz, P. Roldán, R. Golcz, C. Moriana, and J. Leute, "Performance of the NeQuick iono model for single-frequency GNSS timing applications," in *2016 European Frequency and Time Forum (EFTF)*. York, UK: IEEE, 2016, pp. 1–4.

[6] K. Davies and G. K. Hartmann, "Studying the ionosphere with the Global Positioning System," *Radio Science*, vol. 32, no. 4, pp. 1695–1703, 1997.

[7] P. Misra, R. I. Abbot, and E. M. Gaposcbkin, "Integrated use of GPS and GLONASS: Transformation between WGS84 and PZ-90," in *Proceedings of ION GPS-96*, Kansas City, MO, September 1996, pp. 307–314.

[8] B. Belabbas and F. Gass, "RAIM algorithms analysis for a combined GPS/GALILEO constellation," in *Proceedings of ION GNSS*, Los Angeles,USA, September 2005, pp. 1781 – 1788.

[9] P. G. Mattos, "Accuracy and availability trials of the consumer GPS/GLONASS receiver in highly obstructed environments," in *Proceedings of ION GNSS*, Portland, OR, September 2011, pp. 2740–2744.

[10] C. Cai, Y. Gao, L. Pan, and W. Dai, "An analysis on combined GPS/COMPASS data quality and its effect on single point positioning accuracy under different observing conditions," *Advances in Space Research*, vol. 54, no. 5, 2014.

[11] E. S. Lohan and K. Borre, "Accuracy limits in multi-GNSS," *IEEE Transactions on Aerospace and Electronic Systems*, vol. 52, no. 5, pp. 159–169, 2016.

[12] P. Misra and P. Enge, *Global Positioning System: Signals, Measurements and Performance*. Lincoln,MA, USA: Ganga-Jamuna, 2006.

[13] P. W. Ward, "Performance comparisons between FLL, PLL and a novel FLL-assisted-PLL carrier tracking loop under RF interference conditions," in *Proceedings of ION GNSS*, Nashville, TN, September 1998, pp. 738–795.

[14] S. Alban, D. M. Akos, and S. M. Rock, "Performance analysis and architectures for INS-aided GPS tracking loops," in *Proccedings of the ION NTM-03*, Anaheim, CA, January 2003, pp. 611 – 622.

[15] D. Gebre-Egziabher, "Doppler aided tracking loops for SRGPS integrity monitoring," in *Proceedings of ION GNSS*, Portland, OR, September 2003, pp. 2562 – 2571.

[16] L. Ries, C. Macabiau, O. Nouvel, and Q. Jeandel, "A software receiver for GPS-IIF L5 signal," in *Proceedings of ION GPS*, Portland, OR, September 2002, pp. 1540 – 2552.

[17] S. U. Qaiser, "Performance analysis of doppler aided tracking loops in modernized GPS receivers," in *Proceedings of ION ITM GNSS*, Savannah,GA, September 2009, pp. 209 – 218.

[18] R. Yang and Y. Morton, "An adaptive inter-frequency aiding carrier tracking algorithm for the mountain-top GPS radio occultation signal," in *Proceedings of the International Technical Meeting (ITM) of The Institute of Navigation (ION)*, Reston, Virginia, January 2018, pp. 412 – 419.

[19] S. H. Delay, C. S. Carrano, K. M. Groves, and P. H. Doherty, "A statistical analysis of GPS L1, L2, and L5 tracking performance during ionospheric scintillation," in *Proc. of ION Pacific PNT Conference 2015*. Honolulu, HI: ION, 2015, p. 1.

[20] J. J. Spilker, "Vector delay lock loop processing of radio location transmitter signals," *U.S. Patent*, vol. 85, no. 5398034, pp. 539 – 553, 1995.

[21] M. Zhodzishsky, S. Yudanov, V. Veitsel, and J. Ashjaee, "Co-op tracking for carrier phase," in *Proc. ION-GPS*. Nashville, TN: Institute of Navigation, 1998, pp. 653 – 664.

[22] T. Pany, R. Kaniuth, and B. Eissfeller, "Deep integration of navigation solution and signal processing," in *Proceedings of Institute of Navigation GPS/GNSS Conference*. Long Beach, CA: Institute of Navigation, 2005, pp. 1095 – 1102.

[23] M. Lashely and D. M. Bevly, "Analysis of discriminator based vector tracking algorithms," in *Proceedings of the Institute of Navigation (NTM)*. San Diego, CA, USA: Institute of Navigation, 2007, pp. 570 – 576.

[24] P. Henkel, K. Giger, and C. Gunther, "Multifrequency, multisatellite vector phase-locked loop for robust carrier tracking," *IEEE Journal of Selected Topics in Signal Processing*, vol. 3, no. 4, pp. 674 – 681, 2009.

[25] P. Senlin, M. Yu, and D. Ruihui, "A multiple-frequency GPS software receiver design based on a vector tracking loop," in *Proceedings of the Institute of Navigation (NTM)*. Myrtle Beach, SC, USA: IEEE, 2012, pp. 495 – 505.

[26] C. Gernot, K. O'Keefe, and G. Lachapelle, "Combined L1/L2C tracking scheme for weak signal environments," in *Proceedings of ION GNSS*, Savannah, GA, September 2008, pp. 1758 – 1772.

[27] D. Megahed, C. O'Driscoll, and G. Lachapelle, "Combined L1/L5 Kalman filter-based tracking for weak signal environments," in *European navigation conference*, Naples, Italy, July 2009, pp. 45 – 56.

[28] R. K. Siddakatte, A. Broumandan, and G. Lachapelle, "Enhanced carrier phase tracking in fading environments using frequency diversity," in *European Navigation Conference (ENC)*. Helsinki, Finland: IEEE, 2016, pp. 1 – 6.

[29] J. Vilà-Valls, P. Closas, and J. T. Curran, "Performance analysis of multi-frequency GNSS carrier tracking for strong ionospheric scintillation mitigation," in *European Signal Processing Conference (EUSIPCO)*. Kos, Greece: European Signal Processing Conference (EUSIPCO), 2017, pp. 2699 – 2703.

[30] K. Borre, D. M. Akos, N. Bertelsen, P. Rinder, and S. H. Jensen, *A software-defined GPS and GALILEO receiver: a single-frequency approach*. Boston: Birkhauser, 2007.

[31] ICD-GPS-200, *NAVSTAR GPS space segment/user segment L1 C/A and L2C interfaces*. USA: ARINC Research Corporation, 2018.

[32] ICD-GPS-705D, *NAVSTAR GPS space segment/user segment L5 interfaces*. USA: ARINC Research Corporation, 2018.

[33] GLONASS-ICD, *Global Navigation Satellite System SIS ICD*. MOSCOW: Russian Institute of Space Device Engineering, 2008.

[34] GALILEO SIS ICD, *GALILEO Open Service Signal in Space Interface Control Document*. Europe: European Union, 2016.

[35] IRNSS SPS ICD, *IRNSS Signal-in-Space Interface Control Document*. India: ISRO, 2017.

[36] QZSS ICD, *Performance Standard (PS-QZSS) and Interface Specification (IS-QZSS)*. Japan: Government of Japan, 2018.

[37] M. Tran and C. J. Hegarty, "Performance evaluations of the new GPS L5 and L2 Civil (L2C) signals," in *Proceedings of ION NTM*, Anaheim, CA, January 2003, pp. 521 – 535.

[38] M. Tran and C. J. Hegarty, "Receiver algorithms for the new civil GPS signals," in *Proceedings of ION NTM*, San Diego, CA, January 2002, pp. 778 – 789.

[39] P. Enge, "GPS modernization: Capabilities of the new civil signals," in *Australian International Aerospace Congress*, Brisbane, August 2003, pp. 1 – 22.

[40] EGSA, "GNSS user technology report," European GNSS Agency, Technical Report ISBN 978-92-9206-029-9, 2016.

[41] D. Odijk, "Ionosphere-free phase combinations for modernized GPS," *Journal of Survey*, vol. 129, no. 4, pp. 165 – 173, 2003.

[42] B. C. Kim and M. V. Tinin, "Potentialities of multi-frequency ionospheric correction in global navigation satellite systems," *Journal of Geodesy*, vol. 85, no. 3, pp. 159 – 169, 2011.

[43] R. Hatch, "Civilian GPS: The benefits of three frequencies," *GPS Solutions*, vol. 3, no. 4, pp. 1 – 11, 2000.

[44] J. Jung, P. Enge, and B. Pervan, "Optimization of cascade integer resolution with three civil GPS frequencies," in *Proceedings of ION GPS*, Salt Lake City, UT, September 2000, p. 2191 – 2200.

[45] K. Wang and M. Rothacher, "Ambiguity resolution for triple-frequency geometry-free and ionosphere-free combination tested with real data," *Journal of Geodesy*, vol. 85, no. 3, pp. 539 – 553, 2013.

[46] M. Cocard, S. Bourgon, O. Kamali, and P. Collins, "A systematic investigation of optimal carrier-phase combinations for modernized triple-frequency GPS," *Journal of Geodesy*, vol. 82, no. 9, pp. 555 – 564, 2008.

[47] C. Gernot, S. K. Shanmugam, K. O'Keefe, and G. Lachapelle, "A novel L1 and L2C combined detection scheme for enhanced GPS acquisition," in *Proc. ION GNSS*, Fort Worth, TX, September 2007, pp. 219 – 230.

[48] E. D. Kaplan and C. J. Hegarty, *Understanding GPS: Principle and Applications*. Norwood: Artech House Inc, 2006.

[49] K. Muthuraman, S. K. Shanmugam, and G. Lachapelle, "Evaluation of data/pilot tracking algorithms for GPS L2C signals using software receiver," in *Proceedings of ION GNSS*, Fort Worth,TX, September 2007, pp. 2499 – 2509.

[50] W. L. Mao, P. H. Lee, and H. Y. Chena, "Bandwidth optimization of carrier/code tracking loops in GPS receiver," in *The 5th IEEE VTS Asia Pacific Wireless Communications Symposium*, Tohoku University, Sendai, June 2008, pp. 1 – 4.

[51] K. Borre and G. Strang, *Algorithms for Global Positioning*. USA: Wellesley-Cambridge Press, 2012.

[52] Y. Bar-Shalom, X. R. Li, and T. Kirubarajan, *Estimation with Applications to Tracking and Navigation*. New York: John Willey and Sons, 2001.

[53] M. S. Grewal and A. P. Andrews, *Kalman Filtering Theory and Practice using MATLAB*. New York: John Willey and Sons, 2008.

[54] P. W. Ward, "Using a GPS receiver monte carlo simulator to predict RF interference performance," in *Proceedings of ION GPS*, Kansas City, MO, September 1997, pp. 1473 – 1482.

[55] R. B. Langley, "Dilution of Precision," in *GPS World*, 1999.

[56] V. Nee and D. J. Richard, "Multipath effects on GPS code phase measurements," *Journal of Institute of Navigation*, vol. 39, no. 2, pp. 177 – 190, 1992.

[57] M. S. Braasch, "GPS multipath model validation," in *Proceedings of ION PLANS*, Atlanta, USA, April 1996, pp. 672 – 678.

[58] M. Z. H. Bhuiyan, E. S. Lohan, and M. Renfors, "A slope-based multipath estimation technique for mitigating short-delay multipath in GNSS receivers," in *Proceedings of IEEE ISCAS*, Paris, France, May 2010, pp. 3573 – 3576.

[59] A. J. V. Dierendonck, P. Fenton, and T. Ford, "Theory and performance of narrow correlator spacing in GPS receivers," in *Proceedings of ION NTM*, San Diego, CA, January 1992, pp. 115 – 124.

[60] J. W. Betz, "Effect of narrowband interference on GPS code tracking accuracy," in *Proccedings of the ION NTM*. Anaheim, CA: Institute of Navigation, 2003, pp. 16 – 27.

[61] P. H. Doherty, S. H. Delay, C. E. Valladares, and J. A. Klobuchar, "Ionospheric scintillation effects in the equatorial and auroral regions," in *Proceedings of the ION GNSS 2000*. Salt Lake City, Utah, USA: Institute of Navigation, 2000.

[62] T. N. Morrissey, K. W. Shallberg, A. J. V. Dierendonck, and M. J. Nicholson, "GPS receiver performance characterization under realistic ionospheric phase scintillation environments," *Radio Science*, vol. 39, no. 2, pp. 1 – 18, 2004.

[63] T. E. Humphreys, M. L. Psiaki, P. M. K. Jr., and B. M. Ledvina, "GPS carrier tracking loop performance in the presence of ionospheric scintillation," in *Proceedings of the ION GNSS 2005*. Long Beach, CA: Institute of Navigation, 2005, pp. 156 – 167.

[64] C. S. Carrano, K. M. Groves, W. J. McNeil, and P. H. Doherty, "Scintillation characteristics across the GPS frequency band," in *Proc. of ION ITM*. Nashville, TN: ION, 2012, pp. 1972 – 1989.

[65] R. Hatch, "The synergism of GPS code and carrier measurements," in *Proceedings of the Third International Geodetic Symposium on Satellite Doppler Positioning*, Las Cruces, NM, February 1982, pp. 1213 – 1232.

[66] P. Y. Hwang, G. A. McGraw, and J. R. Bader, "Enhanced differential GPS carrier smoothed code processing using dual frequency measurements," *Navigation*, vol. 46, no. 2, pp. 127 – 137, 1999.

[67] G. A. McGraw, "Generalized divergence-free carrier smoothing with applications to dual frequency differential GPS," *Navigation*, vol. 56, no. 2, 2009.

[68] F. M. Gernot, M. G. Petovello, and G. Lachapelle, "Combined acquisition and tracking methods for GPS L1 C/A and L1C signals," *International Journal of Navigation and Observation*, vol. 2010, no. 190465, p. 19, 2010.

[69] R. L. S. Bisnath, "High-precision positioning with a single GPS receiver," in *Proc. of ION GPS*. Washington, D.C.: ION, 2001, pp. 2585 – 2595.

[70] B. L. Z. Zhou, "Optimal doppler-aided smoothing strategy for GNSS navigation," *GPS Solutions*, vol. 21, no. 1, pp. 197 – 210, 2017.

[71] J. Vilà-Valls, P. Closas, M. Navarro, and C. Fernández-Prades, "Are PLLs dead? a tutorial on Kalman filter-based techniques for digital carrier synchronization," *IEEE Aerospace and Electronic Systems Magazine*, vol. 32, no. 7, pp. 28 – 45, 2017.

[72] A. H. Jazwinski, "Adaptive filtering," *Journal Automatica*, vol. 5, no. 4, pp. 475 – 485, 1969.

[73] M. Psiaki and H. Jung, "Extended Kalman filter methods for tracking weak GPS signals," in *Proceedings of the 15th ITM-ION*. Portland, OR: Institute of Navigation, 2002, pp. 2539 – 2553.

[74] A. Patapoutian, "On phase-locked loops and Kalman filters," *IEEE Transactions on Communications*, vol. 47, no. 5, p. 670 – 672, 1999.

[75] R. G. Brown and P. Y. C. Hwang, *Introduction to Random Signals and Applied Kalman Filtering.* New York: John Willey and Sons, 1997.

[76] M. S. Mohan, R. M. O. N. Naik, M. R. Gemson, and Ananthasayana, "Introduction to the Kalman filter and tuning its statistics for near optimal estimates and Cramér-Rao bound," IIT Kanpur, Report TR/EE2015/401, 2015.

[77] A. H. Mohamedand and K. P. Schwarz, "Adaptive Kalman filtering for INS/GPS," *Journal of Geodesy*, vol. 73, no. 4, p. 193 – 203, 1993.

[78] R. K. Mehra, "On the identification of variance and adaptive Kalman filtering," *IEEE Transactions on Automatic Control*, vol. 15, no. 2, pp. 175 – 184, 1970.

[79] S. Satyanarayana, D. Borio, and G. Lachapelle, "C/N0 estimation: Design criteria and reliability analysis under Global Navigation Satellite System (GNSS) weak signal scenarios," *IET Radar, Sonar and Navigation*, vol. 6, no. 2, pp. 81 – 89, 2012.

[80] J. H. Won, "A novel adaptive digital phase lock loop for modern digital GNSS receivers," *IEEE Communications Letters*, vol. 17, no. 2, pp. 393 – 396, 2014.

[81] C. O'Driscoll and G. Lachapelle, "Comparison of traditional and Kalman filter based tracking architectures," in *Proc. of European Navigation Conference 2009 (ENC09)*. Naples, Italy: European Navigation Conference 2009, 2009, pp. 100 – 110.

[82] J. H. Won, T. Pany, and B. Eissfeller, "Characteristics of Kalman filter approach for signal tracking loop of GNSS receiver," *IEEE Aerospace and Electronics Systems*, vol. 48, no. 4, pp. 3671 – 3681, 2012.

[83] V. Lucas-Sabola, G. Seco-Granados, J. A. López-Salcedo, and J. A. García-Molina, "GNSS IoT positioning: From conventional sensors to a cloud-based solution," in *Inside GNSS*, June 2018, pp. 1 – 4.

Tampereen teknillinen yliopisto
PL 527
33101 Tampere

Tampere University of Technology
P.O.B. 527
FI-33101 Tampere, Finland

ISBN 978-952-15-4288-6
ISSN 1459-2045